nature methods

Article

https://doi.org/10.1038/s41592-025-02908-8

4Pi-SIMFLUX: 4Pi single-molecule localization microscopy with structured illumination

Received: 20 March 2025

Accepted: 15 October 2025

Qian Wang[1,2,6], Bei Zheng[2,3,6], Zijing Yu[2], Yajing Zhan[2], Qiuyang Dai[2], Xulong Wang[2,4], Shuxin Li[2], Yu Qiao[1,2], Linlin Chen[2], Xiaochun Yu[2,3,5], Yu Lin[4] & Yongdeng Zhang[2,3,5]

Single-molecule localization microscopy (SMLM) has transformed biological imaging by enabling nanoscale visualization of intricate subcellular structures. However, conventional three-dimensional SMLM techniques typically exhibit lower axial resolution than lateral resolution, hindering isotropic investigations. Interferometric approaches, such as 4Pi-SMLM, enhance axial resolution by approximately fivefold through dual-objective coherent fluorescence detection, surpassing lateral resolution. Here we present 4Pi-SIMFLUX, which integrates structured illumination into 4Pi-SMLM to double its lateral resolution, achieving near-isotropic three-dimensional localization precision of 2–3 nm. We demonstrate that 4Pi-SIMFLUX breaks the 10-nm resolution barrier in biological samples, resolving microtubule ultrastructure and nuclear pore complexes with exceptional detail and clarity, while accounting for label size and localization density. Furthermore, it enables simultaneous multicolor imaging for interrogating multiple cellular components and high-fidelity, whole-cell visualization that captures comprehensive spatial organization. 4Pi-SIMFLUX effectively bridges the axial–lateral resolution gap, establishing a robust tool for molecular-scale imaging in complex cellular environments.

Resolving subcellular architecture through three-dimensional (3D) fluorescence microscopy at the molecular scale (<5 nm) remains a formidable challenge in cell biology. Single-molecule localization microscopy (SMLM) offers unparalleled potential in this endeavor, enabling precise nanoscale investigation of ultrastructural details across diverse biological contexts[1]. However, conventional 3D-SMLM methods suffer from anisotropic resolution, with axial localization precision that is typically 2–3 times inferior to lateral precision[2] (Extended Data Fig. 1a). Interferometric methods address this disparity by improving axial resolution approximately fivefold, achieved either through coherent fluorescence detection in a dual-objective setup, as in 4Pi-SMLM[3–6], or via axial interference fringes in a single-objective configuration, such as ROSE-Z[7]. This enhancement not only surpasses the lateral resolution of conventional 3D-SMLM but also introduces a new form of resolution anisotropy, shifting the performance bottleneck to the lateral dimension (Extended Data Fig. 1b). The advent of MINFLUX presents an innovative strategy for advancing the SMLM precision limit by employing patterned illumination with an intensity minimum, which facilitates more efficient extraction of positional information[8]. Although initial MINFLUX implementations

---

[1]College of Life Sciences, Zhejiang University, Hangzhou, China. [2]State Key Laboratory of Gene Expression, School of Life Sciences, Westlake University, Hangzhou, China. [3]Westlake Laboratory of Life Sciences and Biomedicine, Hangzhou, China. [4]Zhejiang University-University of Illinois Urbana-Champaign Institute, Zhejiang University, Haining, China. [5]Research Center for Industries of the Future, Westlake University, Hangzhou, China. [6]These authors contributed equally: Qian Wang, Bei Zheng. e-mail: zhangyongdeng@westlake.edu.cn

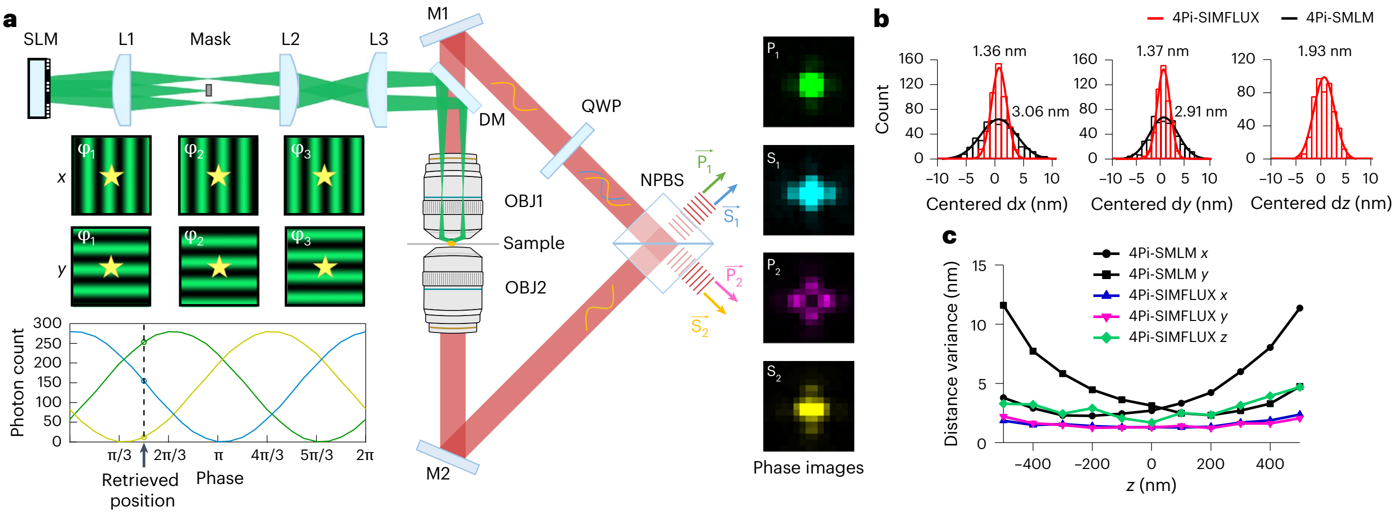

Fig. 1 | Principle and validation of 4Pi-SIMFLUX. a, Schematic of 4Pi-SIMFLUX. Excitation: an SLM modulates a laser to generate three phase-shifted illumination patterns along the *x* or *y* direction at the sample plane. Emission: fluorescence is coherently collected by two opposing objectives to generate four-phase images. Lateral positions are estimated from photon counts in images acquired with three illumination patterns per direction, while axial positions are determined from photon counts in the four-phase images. **b**, Histograms of the relative 3D positions between two 40-nm fluorescent beads in each direction, reconstructed with 4Pi-SIMFLUX and 4Pi-SMLM. The photon counts for the two beads were 5,012 ± 145 and 5,631 ± 170 (mean ± s.d.), respectively. **c**, Distance variance in s.d. of two 40-nm fluorescent beads imaged at different depths, reconstructed with 4Pi-SIMFLUX and 4Pi-SMLM. The photon counts for the two beads were 6,756 ± 392 and 5,302 ± 280 (mean ± s.d.), respectively. L, lens; M, mirror; DM, dichroic mirror; OBJ, objective; QWP, quarter-wave plate; NPBS, nonpolarizing beamsplitter.

localized one molecule at a time using doughnut-shaped illumination, subsequent extensions (hereafter termed SIMFLUX) adopted striped illumination patterns for parallelized localization, albeit with reduced resolution gains[9–12].

In this work, we introduce 4Pi-SIMFLUX, a super-resolution microscope that integrates SIMFLUX with 4Pi-SMLM to double lateral precision while maintaining excellent axial performance, achieving near-isotropic 3D nanoscale resolution (Extended Data Fig. 1c,d and Supplementary Note 1). We demonstrate that 4Pi-SIMFLUX attains near-isotropic 2–3-nm localization precision in fixed cells, resolving the hollow structure of bundled microtubules with exceptional clarity. Furthermore, the system successfully distinguishes adjacent Nup96 proteins, revealing all 32 copies in a structural average. These results confirm that 4Pi-SIMFLUX delivers sub-10-nm 3D resolution in biological samples, accounting for label size and localization density. The versatility of this approach is further highlighted by its capacity for simultaneous two-color imaging and high-quality, whole-cell visualization across diverse biological samples. Collectively, these capabilities underscore the transformative potential of 4Pi-SIMFLUX for elucidating molecular-scale details of cellular architecture.

Results

Implementation and characterization of 4Pi-SIMFLUX

The basic principle of 4Pi-SIMFLUX is illustrated in Fig. 1a, with the microscope's optomechanical design detailed in Extended Data Figs. 2 and 3 and Supplementary Video 1. In the excitation path, a high-speed spatial light modulator (SLM) generates dynamic striped illumination patterns at the sample plane by modulating a laser beam (Extended Data Fig. 2a). Each illumination direction employs three phase-shifted patterns with 2π/3 increments (φ_1, φ_2 and φ_3), resulting in six distinct patterns (Extended Data Fig. 4). In the emission path, fluorescence signals are coherently collected by dual objectives, with four-phase images (P_1, S_1, P_2 and S_2) each corresponding to a specific phase delay (0, π/2, π and 3π/2) captured simultaneously (Extended Data Fig. 2b). By exploiting interference effects in both excitation and emission paths, 4Pi-SIMFLUX concurrently enhances lateral and axial precision, achieving near-isotropic nanoscale 3D resolution (Extended Data Fig. 1c).

Next, we developed a reconstruction pipeline integrating SIMFLUX and 4Pi-SMLM algorithms (Extended Data Fig. 5 and Supplementary Note 2). As described above, 4Pi-SIMFLUX generates 24 sub-images (six *x*–*y* patterns × four *z* phases). Two deformable mirrors introduced a slight astigmatism, resulting in elliptical emission point spread function (PSF) patterns. For 3D-SMLM, the 24 sub-images were registered and summed, and rough *x*–*y*–*z* positions were estimated using astigmatism-based maximum likelihood estimation (MLE) fitting with an elliptical Gaussian PSF model[13,14]. For 4Pi-SMLM, the six *x*–*y* sub-images were summed to form four *z* phase images. The Gaussian-weighted zeroth moment intensities of these images were computed to estimate the axial phases of the molecules[4], and a ridge-finding algorithm was applied to unwrap the phases and determine precise *z* positions[3]. For 4Pi-SIMFLUX, the four *z* phase images were summed to form six *x*–*y* sub-images, and the photon number from each sub-image was then used to calculate the phases in the *x*–*y* directions. A linear regression procedure aligned the phases with the rough *x*–*y* positions to obtain precise *x*–*y* coordinates[12]. This unified pipeline enabled a quantitative comparison of 3D-SMLM, 4Pi-SMLM and 4Pi-SIMFLUX using identical data under the same conditions.

To experimentally validate 4Pi-SIMFLUX, we imaged 40-nm fluorescent beads and determined their relative 3D positions to quantify localization precision at varying depths. The samples were sandwiched between two coverslips and mounted in a custom-designed holder (Extended Data Fig. 6). The striped illumination pattern exhibited spatial periods of 210 nm (*x* axis) and 209 nm (*y* axis) (Extended Data Fig. 7a,b), with modulation contrasts of 0.91 and 0.92, respectively (Extended Data Fig. 7c,d). 4Pi-SIMFLUX achieved sub-2-nm localization precision in all three dimensions at the focal plane with a photon budget of around 5,500, demonstrating a twofold improvement in lateral precision compared to 4Pi-SMLM (Fig. 1b). Moreover, it maintained near-isotropic localization precision of 2–3 nm at different axial positions with a photon budget of around 6,000 (Fig. 1c).

4Pi-SIMFLUX resolved bundled microtubules

We then benchmarked 4Pi-SIMFLUX on biological samples. Given that its localization precision approaches the molecular scale, label size and

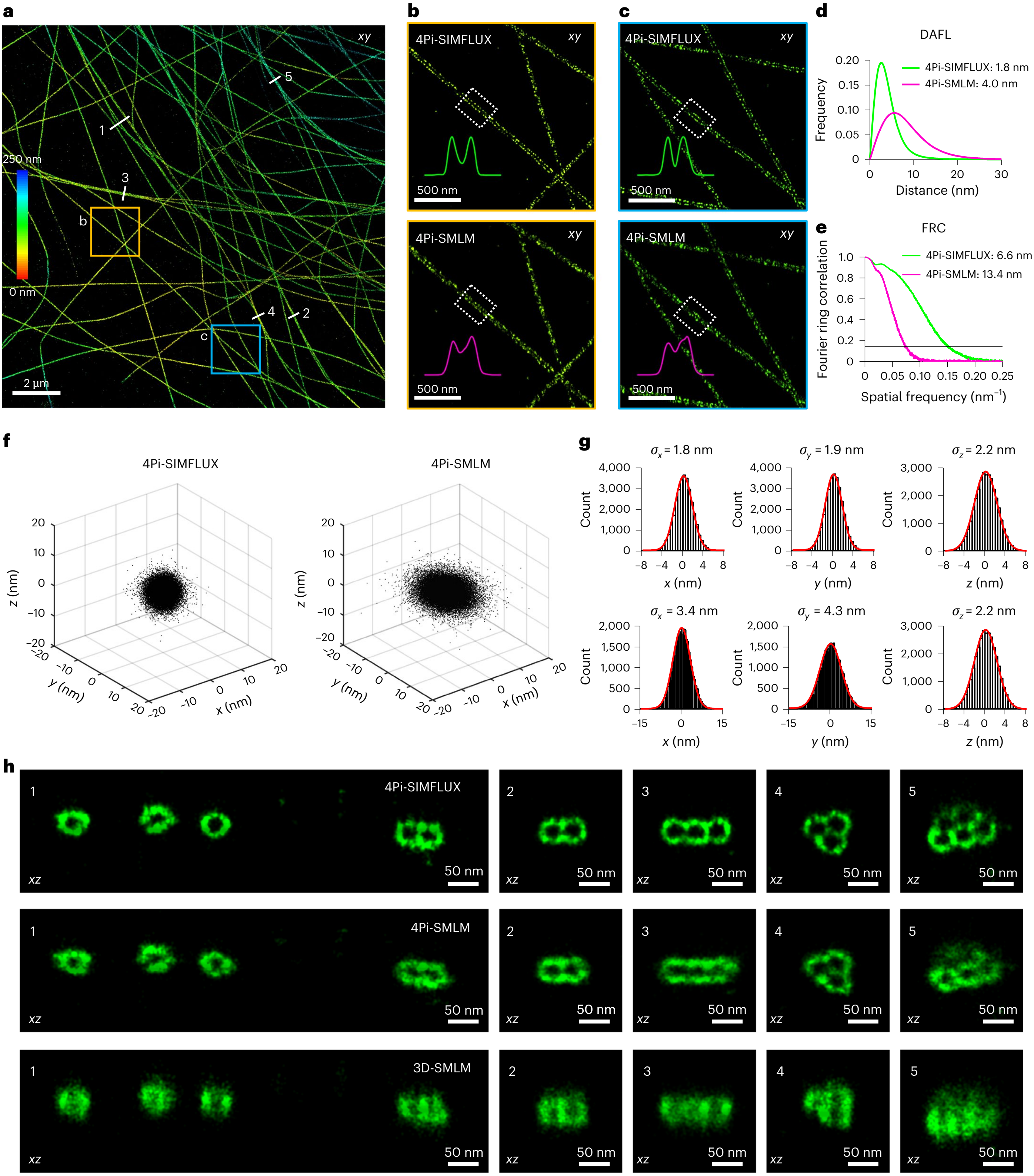

Fig. 2 | 4Pi-SIMFLUX imaging of microtubules. **a**, 4Pi-SIMFLUX image of microtubules in a fixed COS-7 cell. **b**,**c**, 10-nm x–y slices of the boxed regions denoted in **a**, reconstructed with 4Pi-SIMFLUX and 4Pi-SMLM. Insets: intensity profiles of the cross-sections denoted by the white dashed boxes. **d**, Histograms of the distances between adjacent-frame localizations for data in **a**, reconstructed with 4Pi-SIMFLUX and 4Pi-SMLM. DAFL localization precision was determined as $\sigma_{\mathrm{loc}} = \mathrm{DAFL}_{max}/\sqrt{2}$. **e**, FRC analysis of the data in **a** reconstructed with 4Pi-SIMFLUX and 4Pi-SMLM. **f**, 3D localization distributions for molecules emitting ≥10 frames, reconstructed with 4Pi-SIMFLUX and 4Pi-SMLM. The photon count for these molecules was 4,025 ± 806 (mean ± s.d). **g**, Histograms of the distributions in **f** were fit with Gaussian functions (top: 4Pi-SIMFLUX; bottom: 4Pi-SMLM), with the standard deviations reported. **h**, Cross-sections at locations denoted by the numbers in **a**, reconstructed with 4Pi-SIMFLUX, 4Pi-SMLM and 3D-SMLM. Color bar denotes depth (**a**–**c**). Scale bars: 2 µm (**a**), 500 nm (**b**,**c**), 50 nm (**h**). Representative results are shown from three independent experiments.

https://doi.org/10.1038/s41592-025-02908-8

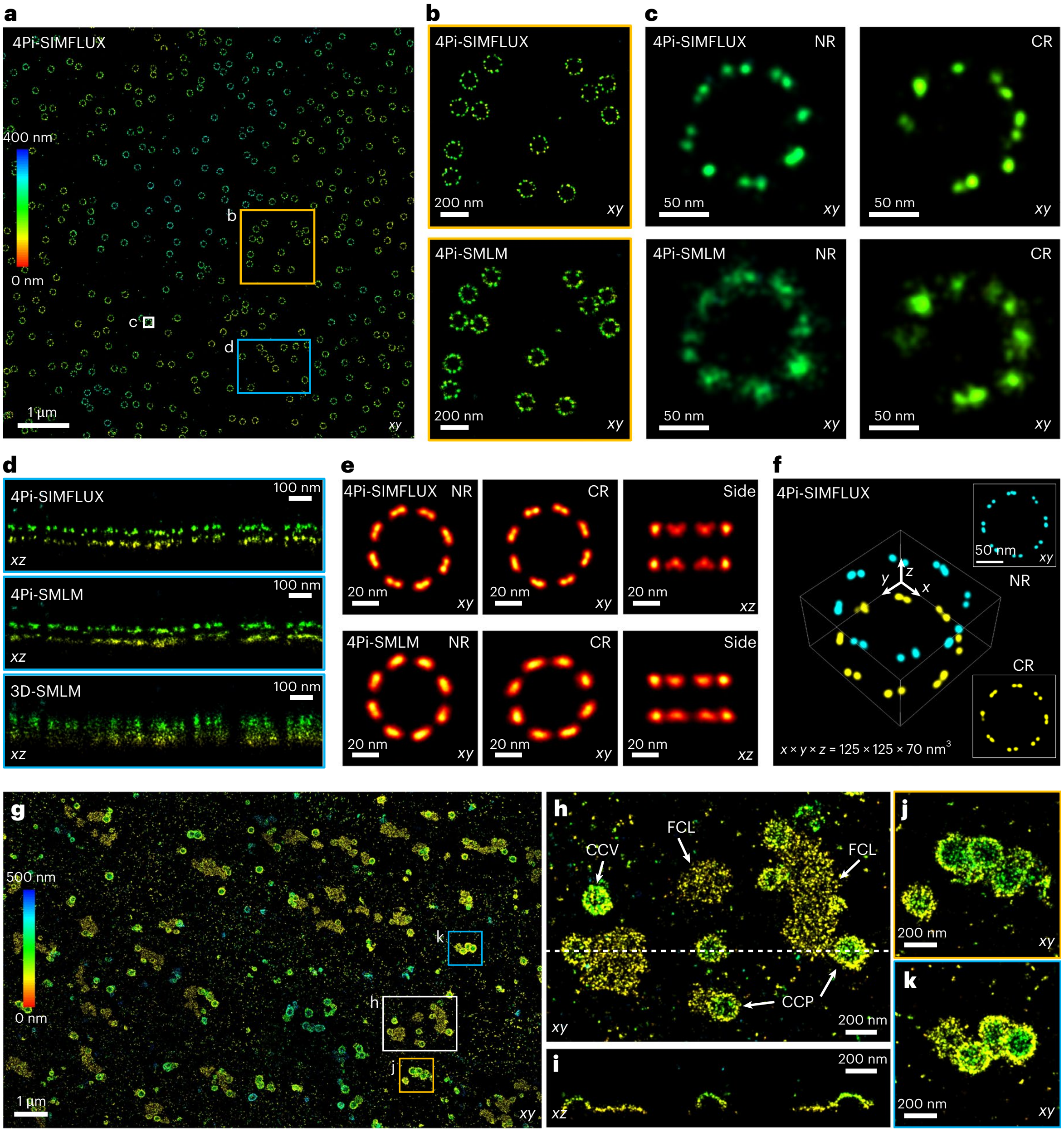

Fig. 3 | 4Pi-SIMFLUX imaging of NPC and clathrin. a, 4Pi-SIMFLUX image of Nup96 in a fixed U-2 OS cell. **b**, Zoom-in images of the regions denoted in **a**, reconstructed with 4Pi-SIMFLUX and 4Pi-SMLM. **c**, NR and CR of the boxed NPC denoted in **a**, reconstructed with 4Pi-SIMFLUX and 4Pi-SMLM. **d**, Side views of the boxed region denoted in **a**, reconstructed with 4Pi-SIMFLUX, 4Pi-SMLM, and 3D-SMLM. **e**, 3D particle averaging of 973 NPCs from the nucleus shown in **a**, reconstructed with 4Pi-SIMFLUX and 4Pi-SMLM. **f**, 3D visualization of the averaged NPC reconstructed with 4Pi-SIMFLUX after cluster analysis. Insets: NR and CR of the averaged NPC structure. **g**, 4Pi-SIMFLUX image of clathrin in a fixed SK-MEL-28 cell. **h**, Zoom-in image of the region denoted in **g**. **i**, Cross-section along the dashed line denoted in **h**. **j**,**k**, Zoom-in images of the regions denoted in **g**. Color bar denotes depth (**a**-**d**, **g**-**k**). Scale bars: 1 µm (**a**, **g**), 200 nm (**b**, **h**, **i**, **j**, **k**), 50 nm (**c**), 100 nm (**d**), 20 nm (**e**), 50 nm (**f** inset). Representative results are shown from three to five independent experiments.

localization density become major constraints for resolution enhancement. To overcome these limitations, we employed nanobodies, which are substantially smaller than conventional primary–secondary antibody pairs, and integrated DNA point accumulation for imaging in nanoscale topography (DNA-PAINT) to achieve high-density localization through transient, replenishable probes. To this end, we developed a labeling strategy combining the ALFA-tag/NbALFA system[15] with speed-optimized DNA-PAINT[16].

First, we generated a COS-7 cell line stably expressing ALFA-tagged Ensconsin, a microtubule-binding protein, immunolabeled with NbALFA conjugated to DNA docking strands, and performed DNA-PAINT imaging (Fig. 2a). To minimize background signal from freely diffusing imager strands, we employed a high-numerical-aperture (NA) oil-immersion objective (1.5 NA) in the upper beam path using a near-total internal reflection fluorescence (TIRF) configuration. 4Pi-SIMFLUX resolved microtubule two-sided structures more distinctly than 4Pi-SMLM (Fig. 2b,c). To quantify the lateral resolution improvement, we employed a method that estimates the localization precision by calculating the distance between adjacent-frame localizations (DAFL)[17], analogous to the nearest-neighbor-based analysis[18] commonly used in SMLM. DAFL analysis revealed a localization precision of 1.8 nm for 4Pi-SIMFLUX, representing a 2.2-fold improvement over 4Pi-SMLM (4.0 nm) (Fig. 2d). Fourier ring correlation (FRC)[19] further confirmed the resolution enhancement (6.6 nm versus 13.4 nm)

https://doi.org/10.1038/s41592-025-02908-8

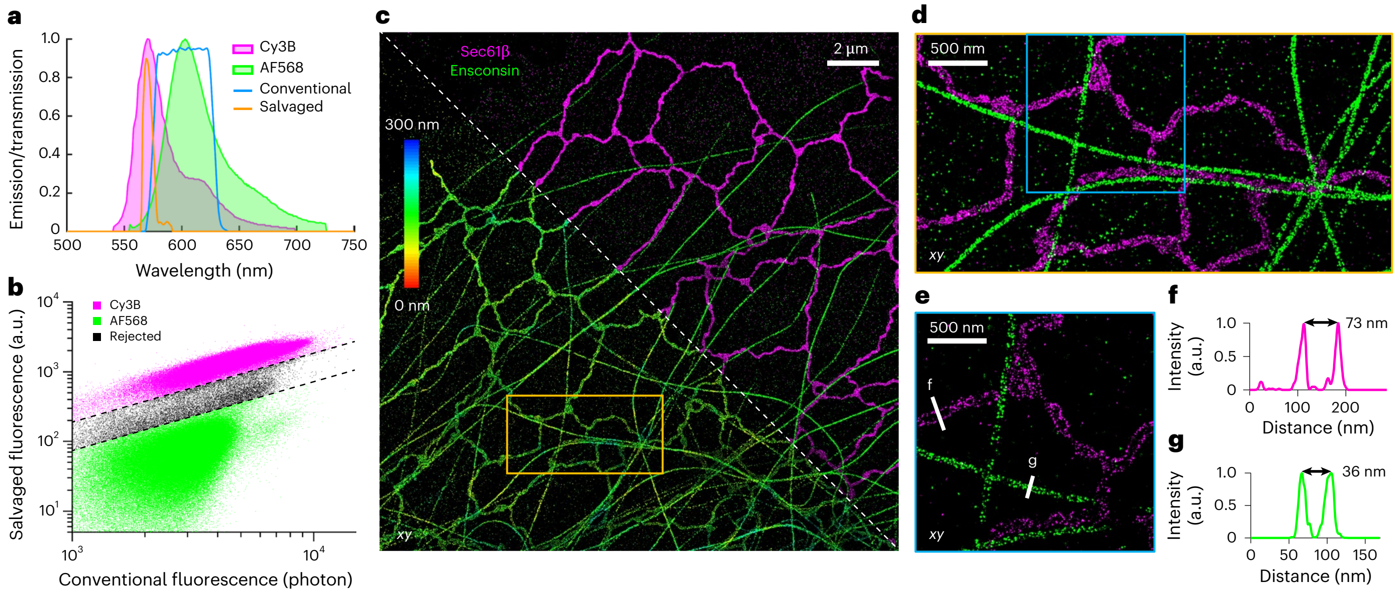

Fig. 4 | Two-color 4Pi-SIMFLUX imaging of ER and microtubules. a, Emission spectra of Cy3B and AF568, and transmission profiles for conventional and salvaged fluorescence. **b**, Scatter plot of salvaged fluorescence versus conventional fluorescence intensities of localized dye molecules from the image shown in **c**, on a logarithmic scale. The two dashed lines indicate the color-assignment threshold and the rejection region. **c**, Two-color 4Pi-SIMFLUX image of ER and microtubules in a fixed COS-7 cell. The lower-left shows the depth color-coded image, and the upper-right shows the merged image of the two labels. **d**, Zoomed-in image of the boxed region denoted in **c**. **e**, A 20-nm-thick *x*–*y* slice of the boxed region denoted in **d**. **f**,**g**, Intensity profiles along the white lines denoted in **e**. Scale bars: 2 µm (**c**), 500 nm (**d**,**e**). Representative results are shown from three independent experiments.

(Fig. 2e). Localization analysis of molecules emitting ≥10 frames demonstrated ~2-nm 3D precision for 4Pi-SIMFLUX in cells (Fig. 2f,g), resolving microtubule ring-like features with greater clarity than 4Pi-SMLM or 3D-SMLM (Fig. 2h).

Revealing the architecture of nuclear pore complexes and clathrin

The nuclear pore complex (NPC) serves as another model structure for quantitative imaging[20]. Nup96, an NPC protein, exhibits eight-fold symmetry with two rings: a nucleoplasmic ring (NR) and a cytoplasmic ring (CR), comprising 32 copies per complex. Notably, two adjacent Nup96 proteins, ~10 nm apart laterally[21,22], remain difficult to resolve even after particle averaging with advanced super-resolution techniques, such as 4Pi-SMLM and MINSTED[23–26]. So far, resolution enhancement by sequential imaging (RESI) stands as the most effective technique for distinguishing Nup96 protein pairs, achieving Ångström resolution by grouping multiple binding events to mimic high photon-count localization[21]. This highlights the inherent challenge of resolving these pairs under photon-limited conditions. To overcome this challenge, we generated a homozygous knock-in U-2 OS cell line where Nup96 is endogenously tagged with the ALFA-tag. We then performed DNA-PAINT imaging on these cells using the aforementioned labeling strategy (Fig. 3a and Supplementary Video 2). Leveraging its twofold lateral resolution improvement, 4Pi-SIMFLUX resolved Nup96 pairs more effectively than 4Pi-SMLM (Fig. 3b,c). With comparable axial resolution, both methods provided better distinction between NR and CR relative to 3D-SMLM (Fig. 3d). Using advanced 3D particle averaging[24,27] of 973 NPCs from a single nucleus, 4Pi-SIMFLUX, but not 4Pi-SMLM, achieved RESI-like quality and resolved Nup96 pairs (Fig. 3e). Further cluster analysis revealed all 32 copies of Nup96 in a structural average (Fig. 3f and Supplementary Video 3), demonstrating that 4Pi-SIMFLUX truly achieved sub-10-nm 3D resolution in biological samples while accounting for the constraints of label size and localization density.

SMLM is generally better suited for imaging fixed samples due to its localization-based principles, and 4Pi-SIMFLUX follows this trend. Nonetheless, dynamic processes can still be inferred from static images when multiple events at distinct stages are captured concurrently. To demonstrate this, we generated a SK-MEL-28 cell line stably expressing ALFA-tagged clathrin light chain and performed 4Pi-SIMFLUX imaging (Fig. 3g and Supplementary Video 4). The imaging revealed characteristic clathrin structures, including flat clathrin lattices (FCLs), clathrin-coated pits (CCPs) and clathrin-coated vesicles (CCVs) (Fig. 3h). Although these observations represent static snapshots, they offer preliminary insights into the dynamic progression of clathrin-mediated endocytosis (Fig. 3i). Notably, we observed multiple instances in which several clathrin-coated pits budded from shared flat lattices, suggesting spatially coordinated clathrin activity within discrete membrane domains (Fig. 3j,k).

Simultaneous two-color 4Pi-SIMFLUX imaging

Beyond high-resolution imaging, multicolor visualization is essential for interrogating spatial relationships, such as colocalization and nanoscale organization, among target proteins and cellular organelles. We previously developed salvaged fluorescence, a technique enabling multicolor imaging with a single excitation laser while minimizing spectral crosstalk and chromatic aberrations[28]. Here we combined salvaged fluorescence with 4Pi-SIMFLUX for multicolor imaging. We identified Alexa Fluor 568 (AF568) as a suitable dye to pair with Cy3B for simultaneous two-color DNA-PAINT imaging with a 560-nm excitation laser (Fig. 4a,b). Overexpression of mEmerald-Sec61β, an endoplasmic reticulum (ER) membrane protein, in COS-7 cells stably expressing ALFA-Ensconsin, facilitated two-color 4Pi-SIMFLUX imaging using nanobodies targeting mEmerald and the ALFA-tag (Fig. 4c,d). The integration of high-precision 4Pi-SIMFLUX with low-crosstalk salvaged fluorescence permitted the simultaneous resolution of hollow ER tubules and microtubules in the same cells (Fig. 4e–g). This approach provides a powerful tool for dissecting the spatial organization of protein complexes and organelle interactions in intact cells.

4Pi-SIMFLUX imaging in whole cells

The combination of speed-optimized DNA-PAINT and near-TIRF illumination limited the imaging depth of 4Pi-SIMFLUX to several hundred

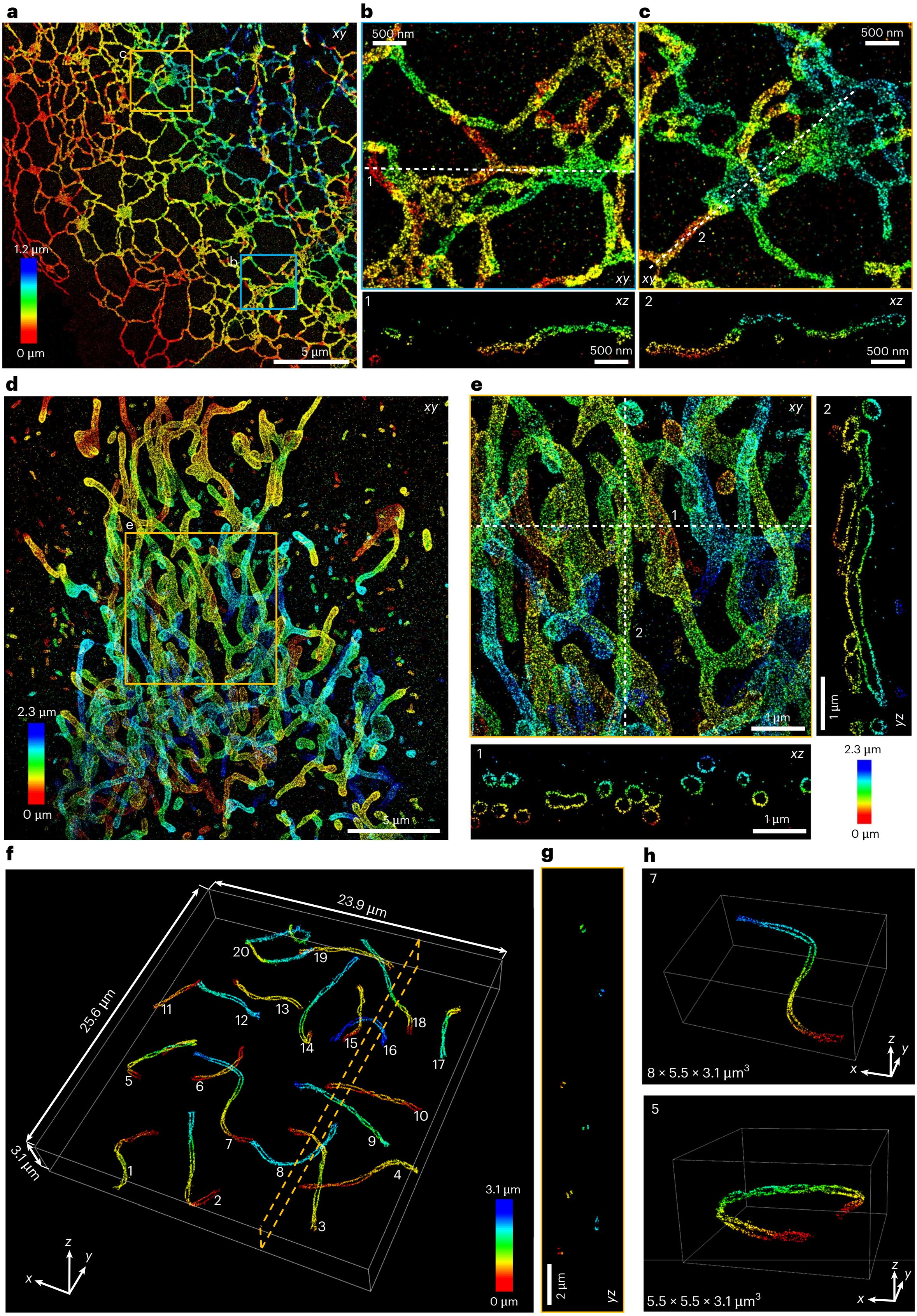

Fig. 5 | Whole-cell imaging with 4Pi-SIMFLUX. a, 4Pi-SIMFLUX image of ER in a fixed COS-7 cell. **b**,**c**, Zoomed-in image of the blue (**b**) or yellow (**c**) boxed region denoted in **a**, and 50-nm-thick *x*–*z* cross-sections along the dashed line denoted by the numbers. **d**, 4Pi-SIMFLUX imaging of mitochondria in HeLa cells overexpressing mCherry-ALFA-OMP25. **e**, Zoomed-in image of the yellow boxed region denoted in **d**, with 100-nm-thick *x*–*z* and *y*–*z* cross-sections along the dashed line denoted by the numbers. **f**, 3D rendering of computationally isolated SC in a fixed mouse spermatocyte imaged with 4Pi-SIMFLUX. **g**, A 100-nm-thick *y*–*z* cross-section at the yellow dashed region in **f**. **h**, Representative 3D views of two SC shown in **f**. The color bar denotes depth. Scale bars: 5 µm (**a**,**d**), 2 µm (**g**), 1 µm (**e**), 500 nm (**b**,**c**). Representative results are shown from three to four independent experiments.

nanometers, restricting its application to cellular structures near the coverslip. To enable deeper imaging within cells and potentially achieve whole-cell imaging, we adopted fluorogenic DNA-PAINT, which reduces background by incorporating a quencher into the imager strands[29]. However, fluorogenic DNA-PAINT was developed for fast binding kinetics, resulting in short on-times that are unfavorable for 4Pi-SIMFLUX. To address this issue, we designed new docking strands with fewer mismatched oligonucleotides to enhance binding affinity and prolong the on-times (Methods). Additionally, we replaced the oil-immersion objective with a silicone oil objective (1.35 NA) in the upper beam path for improved interference contrast (Methods) and employed highly inclined and laminated optical sheet (HILO) illumination.

The low background of fluorogenic DNA-PAINT, combined with HILO illumination, facilitated 4Pi-SIMFLUX imaging of the ER in fixed COS-7 cells over a thickness of ~1.2 µm, roughly matching the imaging depth of the objective (Fig. 5a and Supplementary Video 5). The ER tubular network was resolved with high resolution and no detectable ghost artifacts (Fig. 5b,c). Next, we imaged the outer membrane of mitochondria in fixed HeLa cells (Fig. 5d and Supplementary Video 6). Four optical sections, acquired at a step size of ~400 nm, were axially aligned to reconstruct the interconnected contour of mitochondria over a depth of 2.3 µm without ghost images (Fig. 5e). Quantitative analysis confirmed that 4Pi-SIMFLUX maintained high spatial resolution across all four optical sections (Extended Data Fig. 8). Finally, we imaged immunolabeled synaptonemal complexes (SC) in a fixed mouse spermatocyte, reconstructed from seven optical sections across a depth of 3.1 µm (Fig. 5f and Supplementary Video 7). 4Pi-SIMFLUX resolved all SC substructures with high clarity, regardless of depth or orientation (Fig. 5g,h). These results validate the excellent capability of 4Pi-SIMFLUX for whole-cell imaging, enabling comprehensive, multi-scale reconstruction of cellular architecture with molecular-level precision, irrespective of organelle orientation or structural complexity.

Discussion

In summary, we developed 4Pi-SIMFLUX, which synergistically integrates structured illumination in the excitation path with interferometric detection in the emission path to enhance the lateral and axial precision of 3D-SMLM by twofold and fivefold, respectively. We demonstrated that 4Pi-SIMFLUX achieves near-isotropic 3D localization precision of 2–3 nm and resolves sub-10 nm structural features across whole mammalian cells (Supplementary Table 1). This advancement elevates nanoscale imaging in complex cellular environments, enabling deeper understanding of biomolecular organization and unlocking new opportunities for structural biology research.

Achieving sub-nm localization precision with 4Pi-SIMFLUX requires further advances, including fluorescent probes with longer on-times and higher photostability, a dedicated microscope room to minimize mechanical drift and stabilize interference patterns, an active sample stabilization module, and advanced algorithms that reach the theoretical performance limit (Supplementary Note 3). Nevertheless, for biological samples, label size remains the major constraint: even nanobodies have a size of 2–4 nm. Therefore, advanced labeling strategies featuring smaller sizes, such as genetic code expansion with unnatural amino acids and click labeling[30,31], hold great potential for enabling 4Pi-SIMFLUX to achieve true molecular-scale imaging at the sub-5-nm level in cellular environments. Additionally, although 4Pi-SIMFLUX provides near-isotropic resolution across whole cells, various alternative approaches with much simpler optical setups have been developed for achieving excellent 3D resolution when biological studies focus on a limited axial range, typically less than 1 µm from the surface. These include techniques based on supercritical angle fluorescence[32,33], metal- or graphene-induced energy transfer[34,35] or direct photometry analysis[36].

4Pi-SIMFLUX has several limitations. First, its high complexity renders it inaccessible to most researchers. Second, the dual-objective configuration precludes conventional mounting methods, such as slides, dishes and welled chambers. Third, it requires fluorophores to remain fluorescent across all six frames, making it suboptimal for techniques such as PALM and dSTORM. Fourth, the complex PSF model necessitates advanced localization algorithms to reach its theoretical resolution limit. Therefore, 4Pi-SIMFLUX is most advantageous when sub-10-nm resolution is required deep within cellular samples, especially for those that are densely labeled.

Currently, two main approaches offer enhanced resolution in SMLM. The first approach increases photon count using chemical methods, exemplified by DNA-PAINT[16,29,37], with RESI representing an extreme case of this strategy[21]. RESI enables molecular-level imaging and quantification with nanometer precision and low requirements for optical setup[38,39]. The second approach focuses on improving photon utilization efficiency through optical techniques, such as MINFLUX[8] and MINSTED[26]. However, MINFLUX-like techniques are limited by a restricted field of view and reduced throughput. These limitations can be mitigated through wide-field implementations, including SIMPLE[11], SIMFLUX[10], ROSE[12], ROSE-Z[7], ModLoc[9] and 4Pi-SIMFLUX, at the expense of more modest improvements in resolution. Notably, DNA-PAINT has been combined with MINFLUX-like and SIMFLUX-like techniques to achieve superior performance[10,12,40]. In particular, recent advances in multiplexed DNA-PAINT now permit simultaneous imaging of up to 30 distinct targets in single cells[41,42]. Coupling this capability with the high resolution with MINFLUX-like and SIMFLUX-like techniques could pave the way for molecular-scale spatial proteomics, offering valuable insights into cellular architecture and function.

Online content

Any methods, additional references, Nature Portfolio reporting summaries, source data, extended data, supplementary information, acknowledgements, peer review information; details of author contributions and competing interests; and statements of data and code availability are available at https://doi.org/10.1038/s41592-025-02908-8.

References

1. Lelek, M. et al. Single-molecule localization microscopy. *Nat. Rev. Methods Primers* **1**, 39 (2021).
2. Liu, S., Huh, H., Lee, S. H. & Huang, F. Three-dimensional single-molecule localization microscopy in whole-cell and tissue specimens. *Annu. Rev. Biomed. Eng.* **22**, 155–184 (2020).
3. Huang, F. et al. Ultra-high resolution 3D imaging of whole cells. *Cell* **166**, 1028–1040 (2016).
4. Aquino, D. et al. Two-color nanoscopy of three-dimensional volumes by 4Pi detection of stochastically switched fluorophores. *Nat. Methods* **8**, 353–359 (2011).
5. Shtengel, G. et al. Interferometric fluorescent super-resolution microscopy resolves 3D cellular ultrastructure. *Proc. Natl Acad. Sci. USA* **106**, 3125–3130 (2009).
6. Bates, M. et al. Optimal precision and accuracy in 4Pi-STORM using dynamic spline PSF models. *Nat. Methods* **19**, 603–612 (2022).
7. Gu, L. et al. Molecular-scale axial localization by repetitive optical selective exposure. *Nat. Methods* **18**, 369–373 (2021).
8. Balzarotti, F. et al. Nanometer resolution imaging and tracking of fluorescent molecules with minimal photon fluxes. *Science* **355**, 606–612 (2017).
9. Jouchet, P. et al. Nanometric axial localization of single fluorescent molecules with modulated excitation. *Nat. Photonics* **15**, 297–304 (2021).
10. Cnossen, J. et al. Localization microscopy at doubled precision with patterned illumination. *Nat. Methods* **17**, 59–63 (2020).

11. Reymond, L. et al. SIMPLE: structured illumination based point localization estimator with enhanced precision. *Opt. Express* **27**, 24578–24590 (2019).
12. Gu, L. et al. Molecular resolution imaging by repetitive optical selective exposure. *Nat. Methods* **16**, 1114–1118 (2019).
13. Huang, B., Wang, W., Bates, M. & Zhuang, X. Three-dimensional super-resolution imaging by stochastic optical reconstruction microscopy. *Science* **319**, 810–813 (2008).
14. Smith, C. S., Joseph, N., Rieger, B. & Lidke, K. A. Fast, single-molecule localization that achieves theoretically minimum uncertainty. *Nat. Methods* **7**, 373–375 (2010).
15. Gotzke, H. et al. The ALFA-tag is a highly versatile tool for nanobody-based bioscience applications. *Nat. Commun.* **10**, 4403 (2019).
16. Strauss, S. & Jungmann, R. Up to 100-fold speed-up and multiplexing in optimized DNA-PAINT. *Nat. Methods* **17**, 789–791 (2020).
17. Dai, M., Jungmann, R. & Yin, P. Optical imaging of individual biomolecules in densely packed clusters. *Nat. Nanotechnol.* **11**, 798–807 (2016).
18. Endesfelder, U., Malkusch, S., Fricke, F. & Heilemann, M. A simple method to estimate the average localization precision of a single-molecule localization microscopy experiment. *Histochem. Cell Biol.* **141**, 629–638 (2014).
19. Nieuwenhuizen, R. P. et al. Measuring image resolution in optical nanoscopy. *Nat. Methods* **10**, 557–562 (2013).
20. Thevathasan, J. V. et al. Nuclear pores as versatile reference standards for quantitative superresolution microscopy. *Nat. Methods* **16**, 1045–1053 (2019).
21. Reinhardt, S. C. M. et al. Ångström-resolution fluorescence microscopy. *Nature* **617**, 711–716 (2023).
22. Schuller, A. P. et al. The cellular environment shapes the nuclear pore complex architecture. *Nature* **598**, 667–671 (2021).
23. Gwosch, K. C. et al. Reply to: assessment of 3D MINFLUX data for quantitative structural biology in cells. *Nat. Methods* **20**, 52–54 (2023).
24. Heydarian, H. et al. 3D particle averaging and detection of macromolecular symmetry in localization microscopy. *Nat. Commun.* **12**, 2847 (2021).
25. Liu, S. et al. Universal inverse modeling of point spread functions for SMLM localization and microscope characterization. *Nat. Methods* **21**, 1082–1093 (2024).
26. Weber, M. et al. MINSTED nanoscopy enters the Ångström localization range. *Nat. Biotechnol.* **41**, 569–576 (2023).
27. Wang, W. et al. Particle fusion of super-resolution data reveals the unit structure of Nup96 in Nuclear Pore Complex. *Sci. Rep.* **13**, 13327 (2023).
28. Zhang, Y. et al. Nanoscale subcellular architecture revealed by multicolor three-dimensional salvaged fluorescence imaging. *Nat. Methods* **17**, 225–231 (2020).
29. Chung, K. K. H. et al. Fluorogenic DNA-PAINT for faster, low-background super-resolution imaging. *Nat. Methods* **19**, 554–559 (2022).
30. Nikic, I. et al. Debugging eukaryotic genetic code expansion for site-specific Click-PAINT super-resolution microscopy. *Angew. Chem. Int. Ed. Engl.* **55**, 16172–16176 (2016).
31. Mihaila, T. S. et al. Enhanced incorporation of subnanometer tags into cellular proteins for fluorescence nanoscopy via optimized genetic code expansion. *Proc. Natl Acad. Sci. USA* **119**, e2201861119 (2022).
32. Bourg, N. et al. Direct optical nanoscopy with axially localized detection. *Nat. Photonics* **9**, 587–593 (2015).
33. Dasgupta, A. et al. Direct supercritical angle localization microscopy for nanometer 3D superresolution. *Nat. Commun.* **12**, 1180 (2021).
34. Chizhik, A. I., Rother, J., Gregor, I., Janshoff, A. & Enderlein, J. Metal-induced energy transfer for live cell nanoscopy. *Nat. Photonics* **8**, 124–127 (2014).
35. Ghosh, A. et al. Graphene-based metal-induced energy transfer for sub-nanometre optical localization. *Nat. Photonics* **13**, 860–865 (2019).
36. Szalai, A. M. et al. Three-dimensional total-internal reflection fluorescence nanoscopy with nanometric axial resolution by photometric localization of single molecules. *Nat. Commun.* **12**, 517 (2021).
37. Jungmann, R. et al. Multiplexed 3D cellular super-resolution imaging with DNA-PAINT and Exchange-PAINT. *Nat. Methods* **11**, 313–318 (2014).
38. Masullo, L. A. et al. Spatial and stoichiometric in situ analysis of biomolecular oligomerization at single-protein resolution. *Nat. Commun.* **16**, 4202 (2025).
39. Honsa, M. et al. Imaging ligand–receptor interactions at single-protein resolution with DNA-PAINT. *Small Methods* **9**, e2401799 (2025).
40. Ostersehlt, L. M. et al. DNA-PAINT MINFLUX nanoscopy. *Nat. Methods* **19**, 1072–1075 (2022).
41. Unterauer, E. M. et al. Spatial proteomics in neurons at single-protein resolution. *Cell* **187**, 1785–1800 (2024).
42. Schueder, F. et al. Unraveling cellular complexity with transient adapters in highly multiplexed super-resolution imaging. *Cell* **187**, 1769–1784 (2024).

Methods

Microscope setup

The 4Pi-SIMFLUX microscope was constructed based on a previously described 4Pi-SMLM system[43], with substantial modifications. The optomechanical design is detailed in Extended Data Figs. 2 and 3. Briefly, the system replaced wide-field illumination in 4Pi-SMLM with structured illumination (Extended Data Fig. 2a) to double the lateral resolution, while retaining the 4Pi fluorescence detection configuration for enhanced axial resolution (Extended Data Fig. 2b). Additionally, it included a focus-lock module for stabilization and the salvaged fluorescence module for multicolor imaging[28] (Extended Data Fig. 2c).

Structured illumination

The illumination path is shown in Extended Data Figs. 2a and 3b–d. A 488-nm laser (Coherent OBIS 488 nm LS 150 mW) and a 560-nm laser (2RU-VFL-P-2000-560, MPB Communications) were modulated by an acousto-optical tunable filter (AOTF, AOTFnC-400.650-TN, AA Opto-Electronic). The laser beam was coupled into a single-mode fiber (SMF, P1-488PM-FC-2, Thorlabs) via a coupling lens (PAF2P-A10A, Thorlabs). The fiber output beam was collimated by lens L1 ($f = 150$ mm, AC254-150-A, Thorlabs) and directed onto a SLM (UHSP1K-488-850, Meadowlark Optics) at a 7.5° incidence angle. A half-wave plate (HWP, AHWP25-VIS-A-M, LBTEK) rotated the laser's polarization to align with the liquid crystal axis of the SLM.

4Pi-SIMFLUX requires orthogonal sine/cosine patterns (0° and 90° orientations) for x–y resolution enhancement. The SLM was programmed to sequentially display six patterns (two orientations × three phases), akin to conventional structured illumination microscopy, but using two orientations instead of three[44]. To avoid aliasing caused by integer-period gratings for 0°/90° orientations, the SLM mounting bracket was designed with a 10° tilt (Extended Data Fig. 3e), enabling SLM projections at 13.2° and 103.2° to generate 0° and 90° fringes on the sample plane. At the Fourier plane of lens L2 ($f = 300$ mm, ACT508-300-A, Thorlabs), a filtering mask removed spurious diffraction orders, retaining only the ±first-order beams. Following this mask, a custom-made four-segmented wave plate (FSW, Fuzhou OYeah Optronics) was used, consisting of two BK7 glass sectors (C1) and two quartz-MgF_2 half-wave plate sectors (C2) with fast axes oriented as indicated by the arrows (Extended Data Fig. 2a). The C1 sectors transmitted p-polarization, while the C2 sectors converted p- to s- polarization. This design ensured that both orthogonal beams, relayed through lenses L3 ($f = 250$ mm, ACT508-250-A, Thorlabs) and L4 ($f = 350$ mm, 49-289, Edmund), maintained s-polarization relative to the objectives, optimizing illumination interference contrast.

A silicone oil-immersion objective (UPLSAPO100XS, 100×/1.35 NA, Olympus) was used in the lower beam path. For the upper path, an oil-immersion objective (UPLAPO100XOHR, 100×/1.5 NA, Olympus) was used to achieve near-TIRF illumination. However, in this configuration, the imaging buffer for DNA-PAINT, which has a refractive index of ~1.33, and the proximity of the cells to the coverslip result in the oil objective collecting more photons compared to the silicone oil objective. This disparity in photon collection reduces interference contrast, thereby compromising axial localization precision. This effect becomes more pronounced during whole-cell imaging. To address this limitation and enhance interference contrast, a second silicone oil-immersion objective was employed for HILO illumination.

Fluorescence detection

The fluorescence detection path is shown in Extended Data Figs. 2b and 3a. To simplify the optical path in the 4Pi cavity, the BK7 and quartz prisms/wedges were removed. Instead, a quarter-wave plate (QWP3, AQWP25-VIS-A-M, LBTEK) was inserted into the upper beam path to introduce a π/2 phase shift between the p- and s-polarized light, generating four-phase images on the sCMOS camera CAM1 (ORCA-Fusion BT, C15440-20UP, Hamamatsu). For two-color imaging, an EMCCD camera CAM2 (iXon Life 897, Andor) was used to collect the salvaged fluorescence.

Focus lock

The focus-lock module is shown in Extended Data Fig. 2c. An 850-nm laser diode (LP850-SF80, Thorlabs) was collimated by lens L15 ($f = 50$ mm, AC254-50A, Thorlabs). After passing through the two objectives, the laser was focused on the camera CAM3 (UI-3240LE-NIR-GL, IDS) via lens L4. A cylindrical lens CY1 ($f = 500$ mm, LJ1144RM-B, Thorlabs) was used to introduce a slight astigmatism. Lateral movement between the objectives resulted in a lateral shift of the laser spot, whereas axial movement altered the shape of the laser spot. The position and shape of the spot were monitored in real time and used as feedback to translate the objectives to their locked positions.

Data acquisition

The synchronization diagram is shown in Extended Data Fig. 4. The SLM was programmed to automatically generate a 6-ms period rectangular wave (5.5 ms on time and 0.5 ms off time). An NI USB-6363 board and LabVIEW 2020 DAQ module were utilized to synchronize this signal with other devices. The SLM output signal was delayed by 1 ms to accommodate the time constraints of SLM pattern switching, resulting in a 4.5-ms exposure time for the sCMOS camera. For two-color imaging, the EMCCD camera acquired an integrated exposure over six sCMOS frames. The AOTF maintained continuous transmission throughout the imaging process.

Illumination grating period

Because the illumination grating pattern cannot be resolved directly due to its spatial period approaching the diffraction limit of the optical system, we adopted the method of solving the illumination wavevector to determine the grating period, as in structured illumination microscopy[44]. For each orientation, the raw data underwent Fourier transformation to transition into the frequency domain. Using the known phase shift information from three phase images, a phase separation matrix was constructed to isolate the zeroth- and ±first-order spectral components. Cross-correlation between the zeroth and +first (or −first) orders was then performed, identifying the magnitude and orientation of the wavevector at the maximum correlation value. To eliminate interference from the central component, a notch filter was applied to suppress the central region of the spectrum. Applying this procedure to both orthogonal orientations yielded grating periods of 210 nm in the x direction and 209 nm in the y direction (Extended Data Fig. 7a,b).

Field of view

The imaging field of view (FOV) of 4Pi-SIMFLUX is 25 × 25 μm^2, with regions of varying sizes shown in different figures for visualization purpose. This FOV is comparable to previously reported values of 20 µm in 4Pi-SMLM[3,28], ~25 µm in ROSE[12]/SIMFLUX[10] and 33 µm in ROSE-Z[7]. 4Pi-SIMFLUX was designed to achieve a FOV of 50 µm. However, in the current setup, software issues with the SLM require the sCMOS camara to operate in external trigger mode, where the camera readout time limits the FOV to 25 µm. Recently, an FOV of 90 µm in diameter for fluorescence interference using water objectives has been reported[44], suggesting that a similar FOV for 4Pi-SIMFLUX is theoretically feasible.

4Pi-SIMFLUX reconstruction

The algorithm workflow is illustrated in Extended Data Fig. 5 and the detailed localization procedure is described in Supplementary Note 2. Lateral localization adopted the reconstruction strategy as previously described[12]. For each illumination pattern, the four-phase images were aligned using an affine transformation matrix (generated from fluorescent beads images) and summed to form a sub-image. Six illumination patterns were used, corresponding to six sub-images (X1, X2, X3, Y1, Y2 and Y3). For SMLM, the six sub-mages were summed, and Gaussian fitting was performed to estimate the rough x–y positions. For SIMFLUX, the photon number from each sub-image was used to calculate the phase and modulation depth in x–y directions. A linear regression procedure was used to align the phase and the rough x–y positions to obtain the precise x–y positions. Axial localization followed standard 4Pi-SMLM procedures[3,43]. The six sub-images were summed to form four- phase images. The photon number from the four-phase images were used to estimate the phases the molecules, which were then converted to axial positions. In this way, interference in illumination (SIMFLUX) improves lateral resolution, while interference in detection (4Pi-SMLM) improves axial resolution, together achieving near-isotropic resolution (4Pi-SIMFLUX). Finally, the drift at minimum entropy[45] algorithm was used for 3D drift correction. Color assignment was done as previously described[28]. Localization filtering is shown in Supplementary Table 2. All 4Pi-SIMFLUX and 4Pi-SMLM images and videos were rendered with Vutara SRX software v.7.0.06 (Bruker). Briefly, intensity-based images were generated using Point Splatting mode with 5–10-nm particle sizes, representing each molecule as a 3D Gaussian distribution with a full width at half maximum corresponding to the particle size. Fiji 1.54f was used to crop images, generate line profiles and perform similar tasks.

Particle averaging

3D particle averaging of the NPC was conducted in two steps: segmentation and averaging. For segmentation, the localization results were imported into SMAP[46]. Using the segmentNPC and NPCsegmentCleanup plugins in SMAP, 973 NPCs were automatically segmented and selected from the nucleus shown in Fig. 3a. For averaging, we followed the previously developed algorithm[27]. Given the statistical variability introduced by the Gaussian mixture model, the process was executed 20 times for data reconstructed with 4Pi-SIMFLUX and 4Pi-SMLM. The averages presented correspond to the result of the best iteration, wherein each point is rendered with a Gaussian of $\sigma = 2$ nm in x, y and z. For cluster analysis, a local outlier factor algorithm in MATLAB R2022b (MathWorks) was used to remove outlier localizations, enabling the visualization of 32 copies of Nup96 proteins (Fig. 3f).

DNA-PAINT docking and imager sequences

DNA oligonucleotides modified with azide, AF568 and Cy3B were purchased from Ningbo Karebay Biochem and GENEray Biotechnology. The docking strands were 5×R6, L5×R2, S4 and LS4. The corresponding imager strands were R6, LR2, P10 and LP10. The sequences of L5×R2, LR2, LS4 and LP10 were synthesized from left-handed DNA to reduce unspecific binding[47]. Fluorogenic probes with longer on-times were optimized for whole-cell imaging. Two orthogonal DNA sequence motifs (LR2 and R6) were used to label targets for two-color imaging. In this work, the docking strands and imager strands used the following nucleotide sequences:

	Oligonucleotide	Nucleotide sequence (5′-3′)
Docking strands	5R6	azide_AACAACAACAACAACAACAA
	L5R2	azide_ACCACCACCACCACCACCA
	S4	CCTTCAACATTTCTTCTAC_azide
	LS4	CCTTCAACATTTCTTCTAC_azide
Imager strands	R6	TTGTTGTT_Cy3B
	R6_AF568	TTGTTGTT_AF568
	LR2	TGGTGGT_Cy3B
	P10	Cy3B_AGAAGTAATGTGGAA_BHQ2
	LP10	Cy3B_AGAAGTAATGTGGAA_BHQ2

Nanobody–DNA conjugation

Nanobodies against ALFA (sdAb anti-ALFA, clone 1G5, cat. no. N1502, lot no. 15220402) and GFP (sdAb anti-GFP, clone 1H1, cat. no. N0302, lot no. 022307) with ectopic cysteines at the C and N terminus were purchased from NanoTag Biotechnologies. These nanobodies were site-specifically conjugated to DNA-PAINT docking strands using a bifunctional crosslinker, as previously described[16,48]. Specifically, nanobodies were concentrated using Amicon spin filters (10-kDa molecular weight cut-off (MWCO); Sigma-Aldrich, cat. no. UFC5010) at 13,000g, with buffer exchange to buffer D (5 mM TCEP (Sigma-Aldrich, cat. no. C4706-2G), PBS (1× PBS, Gibco, cat. no. 10010023), 1 mM EDTA (Invitrogen, cat. no. 91222915), pH 6.8). Disulfide bonds were reduced by incubating nanobodies in buffer D for 30 min in the dark at 4 °C with shaking. TCEP was removed using 10-kDa Amicon filters, and the buffer was exchanged to PBS. Free cysteines were reacted with a 20-fold molar excess of bifunctional DBCO–PEG$_4$–Maleimide (Sigma-Aldrich, cat. no. 760676) crosslinker for 4 h in the dark at 4 °C on a shaker. Unreacted crosslinker was removed via 10-kDa Amicon filters. A copper-free click reaction was performed by adding azide-modified DNA in a fivefold molar excess to DBCO-nanobodies, followed by overnight incubation at 4 °C. Unconjugated azide–DNA and protein were removed sequentially by size-exclusion chromatography (Superdex 75 10/300 GL, GE Healthcare) and anion-exchange chromatography (Resource Q 1-ml column) using an ÄKTA Pure system. The nanobody–DNA conjugates (NbALFA-L5R2, NbALFA-5R6, NbALFA-LS4 and NbGFP-L5R2) were adjusted to 10 μM in storage buffer and stored at −20 °C.

Conjugation of secondary antibodies with docking strands

Docking strands were conjugated to secondary goat anti-mouse antibodies (Jackson ImmunoResearch, cat. no. 115-005-146, lot no. 171417) as previously described[29]. Briefly, DBCO–sulfo–NHS ester (Sigma-Aldrich, cat. no. 762040) crosslinker was added to the antibodies at a 20-fold molar excess in the dark at 4 °C overnight. Purification of the conjugated antibodies was performed by ZEBA spin desalting column (7-kDa MWCO, Thermo Fisher Scientific, cat. no. 89882) for removing the excess crosslinker. Azide-modified DNA (docking strand S4) was added to the purified antibody–crosslinker solution at a 10-fold molar excess and incubated in the dark at room temperature for 1 h. Subsequently, Amicon spin filters (100-kDa MWCO, Sigma-Aldrich, cat. no. UFC5100) were used to remove unreacted azide–DNA and the antibody–DNA conjugate (20 μM) was stored at −20 °C in storage buffer (50% glycerol (Sigma-Aldrich, cat. no. V900122) in PBS).

Plasmid construction

The following plasmids were used: mEmerald-Sec61β, EGFP-OMP25 and mEmerald-Ensconsin[44]. For ER labeling, we overexpressed mEmerald-Sec61β, and constructed mEmerald-ALFA-Sec61β by inserting an ALFA-tag to the N terminus of Sec61β. For microtubule labeling, we constructed oxStayGold-ALFA-Ensconsin by replacing the mEmerald gene with the oxStayGold gene from pcDNA3/er-(n2)oxStayGold(c4) (Addgene, plasmid no. 185822) in mEmerald-Ensconsin. An ALFA-tag was inserted at the N terminus of Ensconsin, and the resulting fragment was cloned into the pSin vector (derived from pSin-GFP (puro), a gift from Q. Xie, Westlake University) using SpeI and BamHI digestion. For clathrin labeling, we constructed mEmerald-Clathrin-ALFA. The clathrin gene was amplified by PCR from Clathrin-mGreenLantern (Addgene, plasmid no. 164462), and the mEmerald gene was obtained from mEmerald-Sec61β. The mEmerald gene, fused to an ALFA-tag at its C terminus, was ligated to the C terminus of clathrin. The fragment was cloned into the pSin vector (derived from pSin-GFP (puro)) using SpeI and BamHI digestion. For mitochondria labeling, we constructed mCherry-ALFA-OMP25 by replacing the EGFP gene with the mCherry gene from mCherry-KDEL (a gift from J. Bewersdorf, Yale University), and an ALFA-tag was inserted at the N terminus of OMP25.

Cell culture and transfection

COS-7 (CRL-1651), HeLa (CCL-2), U-2 OS (HTB-96) and SK-MEL-28 (HTB-72) cell lines were purchased from the American Type Culture

Collection (ATCC). COS-7 cells were cultured in DMEM (Gibco, cat. no. C11965500CP), U-2 OS cells in McCoy's 5A medium (Gibco, cat. no. 16600-082), and SK-MEL-28 cells in EMEM (ATCC, cat. no. 30-2003). All media were supplemented with 10% fetal bovine serum (Sigma-Aldrich, cat. no. F8318) and 1% penicillin–streptomycin (Gibco, cat. no. 15140122). Cells were maintained at 37 °C with 5% CO_2 and routinely tested for mycoplasma contamination. Before cell plating, high-precision coverslips (Marienfeld, cat. no. 0117650) were cleaned by immersion in 1 M KOH (Sigma-Aldrich, cat. no. 484016) and sonicated for 15 min. The coverslips were subjected to three 10-min sonication cycles in ddH_2O, sterilized with 100% ethanol (J&K Scientific, cat. no. 258449) for 1 min, and coated with poly-L-lysine (Sigma-Aldrich, cat. no. P4707). On the day before transfection, ~1×10^5 cells were seeded on coverslips in a six-well plate. Transient transfections were performed using Lipofectamine 3000 (Thermo Fisher Scientific, cat. no. L3000015) according to the manufacturer's instructions, with 1 μg of DNA per well of a six-well plate.

Stable cell-line generation

To generate stable COS-7 cell lines expressing oxStayGold-ALFA-Ensconsin and stable SK-MEL-28 cell lines expressing mEmerald-Clathrin-ALFA, HEK293T (CRL-3216) cells were co-transfected with a lentiviral transfer plasmid (pSin-oxStayGold-ALFA-Ensconsin or pSin-mEmerald-Clathrin-ALFA) and packaging plasmids psPAX2 (Addgene, plasmid no. 12260) and pMD2.G (Addgene, plasmid no. 12259) using Lipofectamine 3000. The transfection mixture was incubated for 12–24 h, after which the medium was replaced with fresh growth medium. Viral supernatants were collected 48–72 h post-transfection, filtered through a 0.45-μm filter (Sigma-Aldrich, cat. no. Z29079) and centrifuged at 600*g* for 5 min. The clarified supernatant was mixed with concentrated viral solution (Biodragon, cat. no. BF06205) in a 4:1 ratio, gently inverted and incubated at 4 °C overnight. The viral solution was centrifuged at 4 °C (4,000*g*, 30 min), and the pellet was resuspended in fresh medium. Cells were transduced with the concentrated viral supernatant in the presence of 8 $\mu g\ ml^{-1}$ polybrene (Beyotime, cat. no. C0351). After 4–6 h of incubation at 37 °C, the viral supernatant was replaced with fresh culture medium. Following 24 h of incubation, cells were selected with 1 $\mu g\ ml^{-1}$ puromycin (Beyotime, cat. no. ST551) for 3–5 days to isolate stable transductants. Stable COS-7 and SK-MEL-28 clones were expanded for experiments. SK-MEL-28 clones expressing mEmerald-Clathrin-ALFA were sorted for low-intensity mEmerald expression using a Sony MA900 cell sorter.

Nup96 CRISPR cell line generation

Single guide RNA (sgRNA) sequences for the generation of U-2 OS Nup96-ALFA-mEGFP CRISPR knock-in cell lines were cloned into pX335-U6-Chimeric_BB-CBh-hSpCas9n (D10A) (Addgene, plasmid no. 42335) via BbsI restriction sites. The donor plasmid PUC57-Nup96-ALFA-mEGFP-donor, synthesized by Tsingke, contains 800 base pair homology arms upstream and downstream of the double-strand break in the Nup96 C terminus. The ALFA and mEGFP sequences were inserted between the homology arms with two linkers (5′-GGAAGTGCTGGGTCTGCAGGCGGATCAGGTACCGGTAGC-3′ and 5′-GGCGGCGGCTCT-3′). The U-2 OS Nup96-ALFA-mEGFP CRISPR knock-in cell lines were generated using CRISPR-Cas9D10A nickase, as described previously[49]. Briefly, paired single-guide RNA sequences for the Nup96 C terminus (sense sgRNA: 5′-GTTGGGAGCCTGTGAGCCCC-3′ and antisense sgRNA: 5′-CAGTTCTCGCAGATAGGACT-3′) were cloned into pX335-U6-Chimeric_BB-CBh-hSpCas9n(D10A). U-2 OS cells were transfected with the two sgRNA plasmids and the donor plasmid (PUC57-Nup96-ALFA-mEGFP-donor). After 7 days, single colonies of GFP-positive cells were sorted using a Sony MA900 multi-application cell sorter. Correct insertion and homozygous integration were confirmed by PCR, DNA sequence analysis, western blot and immunofluorescence.

Microtubule labeling

COS-7 stable cells overexpressing oxStayGold-ALFA-Ensconsin were seeded on coverslips in a six-well plate. Following overnight incubation, the cells were prefixed with pre-warmed 0.3% glutaraldehyde (GA, Electron Microscopy Sciences, cat. no. 16020) and 0.25% Triton X-100 (Sigma-Aldrich, cat. no. T8787) in cytoskeletal buffer (CB buffer: 10 mM MES (Sigma-Aldrich, cat. no. M3671-50G), 150 mM NaCl (Sigma-Aldrich, cat. no. S5886-5KG), 5 mM $MgCl_2$ (Sigma-Aldrich, cat. no. M2393-500G), 5 mM EGTA (Sigma-Aldrich, cat. no. 03777-10 g), 5 mM glucose (Sigma-Aldrich, cat. no. G8270-1kg), pH 6.1) for 2 min, followed by fixation with pre-warmed 2% GA in CB buffer for 10 min. After fixation, the cells were quenched with freshly prepared 0.1 M NH_4Cl (Sigma-Aldrich, cat. no. A9434) in PBS for 5 min. The cells were then rinsed three times with PBS. Subsequently, the cells were blocked and permeabilized with blocking buffer A (3% BSA (Jackson ImmunoResearch, cat. no. 001-000-162) and 0.2% Triton X-100 in PBS) for 1 h at room temperature. For labeling, the cells were incubated with anti-ALFA nanobody probes with docking strands L5R2 (NbALFA-L5R2, 20 nM) in dilution buffer (1% BSA and 0.2% Triton X-100 in PBS) at 4 °C overnight. Finally, the cells were washed with wash buffer (0.1% Triton X-100 in PBS) for three 5-min washes, followed by two 10-min washes with PBS. Before introducing the imager solution (LR2, 200 pM), the samples were washed with buffer C (PBS, 1 mM EDTA, 500 mM NaCl, 0.02% Tween-20 (Sigma-Aldrich, cat. no. P1379-500ML), pH 7.4) for 5 min.

NPC labeling

U-2 OS cells expressing Nup96-ALFA-mEGFP were seeded on coverslips and cultured for 48 h. The cells were fixed with pre-warmed 2.4% paraformaldehyde (PFA, Electron Microscopy Sciences, cat. no. 15710) in PBS for 30 min at room temperature and quenched with 0.1 M NH_4Cl in PBS for 5 min. Subsequently, the cells were washed four times with PBS, for 30 s, 60 s and twice for 5 min. Permeabilization and blocking were performed simultaneously in blocking buffer B (3% BSA and 0.25% Triton X-100 in PBS) for 2 h at room temperature. For labeling, the cells were incubated with NbALFA-L5R2 probes (20 nM) in dilution buffer at 4 °C overnight. The following day, the samples were washed three times with wash buffer for 5 min each, and twice with PBS for 10 min each. Before introducing the imager solution (LR2, 300 pM), samples were washed with buffer C for 5 min.

Clathrin labeling

SK-MEL-28 stable cells overexpressing mEmerald-Clathrin-ALFA were cultured on coverslips for 24 h. The cells were fixed with 3% PFA in CB buffer for 20 min at room temperature and quenched with 0.1 M NH_4Cl in PBS for 5 min, followed by three 5-min washes with PBS. Nonspecific binding was blocked by incubation with blocking buffer A for 1 h. Cells were incubated with NbALFA-L5R2 probes (20 nM) in dilution buffer at 4 °C overnight. Unbound probes were removed by washing the samples three times with wash buffer for 5 min each, followed by two washes with PBS for 10 min each. Before introducing the imager solution (LR2, 200 pM), the samples were washed with buffer C for 5 min.

Two-color sample labeling

COS-7 stable cells expressing oxStayGold-ALFA-Ensconsin were cultured on coverslips for 24 h, then transfected with mEmerald-sec61β and cultured for an additional 24 h. Subsequently, the cells were fixed with 3% PFA and 0.1% GA in PBS for 15 min at room temperature and quenched with 0.1 M NH_4Cl in PBS for 5 min, followed by three 5-min washes in PBS. Nonspecific binding was blocked by incubation with blocking buffer A for 1 h at room temperature. The cells were then incubated with NbALFA-5R6 and NbGFP-L5R2 probes (25 nM each) in dilution buffer overnight at 4 °C. Post-labeling, the cells were washed three times with wash buffer for 5 min each, followed by two washes with PBS for 10 min each. Before introducing the imager solution (LR2, 350 pM; R6_AF568, 50 pM), the samples were washed with buffer C for 5 min.

ER and mitochondria labeling

COS-7 and HeLa cells transfected with mEmerald-ALFA-Sec61β and mCherry-ALFA-OMP25 were fixed with 3% PFA and 0.1% GA in PBS for 15 min at room temperature. The samples were quenched with 0.1 M NH_4Cl for 5 min, followed by three 5-min washes in PBS. The samples were then blocked and permeabilized with blocking buffer A for 1 h at room temperature. For labeling, the cells were incubated with NbALFA-LS4 (20 nM) in dilution buffer overnight at 4 °C. Then, the cells were washed three times with wash buffer for 5 min each, followed by two 10-min washes with PBS. Before introducing the imager solution, the samples were washed with buffer E (PBS, 500 mM NaCl, 20 mM Na_2SO_3 (Sigma-Aldrich, cat. no. 71988-250G), 1 mM Trolox (Sigma-Aldrich, cat. no. 238813-1G, pH 7.4) for 5 min.

Synaptonemal complex samples

Male C57BL/6 J mice (JAX, 000664) were laboratory bred or purchased from the animal source center at Westlake University. All experimental procedures were approved by the Institutional Animal Care and Use Committee (IACUC) at Westlake University. Mice were housed in a specific pathogen-free facility at the Laboratory Animal Center of Westlake University. Environmental conditions were carefully controlled and monitored, maintaining a standard 12-h light/dark cycle, ambient temperature between 22 and 26 °C, relative humidity levels of 40–70% and continuous access to standard laboratory food and water. The samples were processed similarly to the previous report[44]. In brief, spermatocytes were isolated from the testes of 3-week-old mice. Testes were gently teased with forceps into buffer I (137 mM NaCl, 2.7 mM KCl, 8 mM Na_2HPO_4 and 2 mM KH_2PO_4; all reagents from Sigma-Aldrich) and mixed 1:1 with buffer II (100 mM sucrose, Sigma-Aldrich). Then, the suspension was filtered through a 70-µm cell strainer. Filtered cells were spread onto glass slides presoaked in buffer III containing 1% PFA and 0.1% Triton X-100, pH 9.2, and dried for 4 h in humidified chambers. The samples were rinsed three times with wash buffer and treated with Image-iT (Invitrogen, cat. no. I36933) for 30 min to enhance signal. After blocking with 3% BSA in PBS for 30 min at room temperature, the samples were incubated with mouse anti-SCP-3 primary antibody (clone D-1, Santa Cruz Biotechnology, cat. no. sc-74569, lot no. J2221, 1:1,000) in 1% BSA in PBS at 4 °C overnight. The cells were then washed three times with wash buffer and incubated with goat anti-mouse-S4 secondary antibody (40 nM) for 1 h at room temperature. Finally, the cells were washed three times for 5 min with wash buffer, followed by two 10-min washes with PBS. Before introducing the imager solution, the samples were washed with buffer E for 5 min.

Sample mounting

The sample mounting is illustrated in Extended Data Fig. 6. The imaging solution containing imager strands in buffer C or buffer E was freshly prepared. The samples were incubated with 40 nm fluorescent beads (Thermo Fisher Scientific, cat. no. F8793; diluted 1:5 × 10^7 in PBS) for 5 min and transferred to the imaging solution for 5 min. A clean coverslip was placed in a custom holder, and 100 µl of imaging solution was spread onto the coverslip. The sample coverslip was placed on top, facing down. Excess imaging solution was removed using Kimwipes. The sample was sealed with two-component silicone glue (Picodent Twinsil, Picodent). After curing for 10–20 min, the samples were transferred to the 4Pi-SIMFLUX system for imaging.

Reporting summary

Further information on research design is available in the Nature Portfolio Reporting Summary linked to this article.

Data availability

An example dataset is available via figshare at https://doi.org/10.6084/m9.figshare.30022948.v1 (ref. 50). Due to the extensive size of the raw data (>1 TB per cell, >50 TB in total), uploading it to an online repository is currently impractical. However, the datasets generated and/or analyzed during the current study are available from the corresponding authors upon request.

Code availability

4Pi-SIMFLUX reconstruction code is available at https://github.com/zhanglab-srm/4Pi-SIMFLUX. The package is licensed under the GNU GPL.

References

43. Wang, J. et al. Implementation of a 4Pi-SMS super-resolution microscope. *Nat. Protoc.* **16**, 677–727 (2021).
44. Ouyang, Z. et al. Elucidating subcellular architecture and dynamics at isotropic 100-nm resolution with 4Pi-SIM. *Nat. Methods* **22**, 335–347 (2025).
45. Cnossen, J., Cui, T. J., Joo, C. & Smith, C. Drift correction in localization microscopy using entropy minimization. *Opt. Express* **29**, 27961–27974 (2021).
46. Ries, J. SMAP: a modular super-resolution microscopy analysis platform for SMLM data. *Nat. Methods* **17**, 870–872 (2020).
47. Geertsema, H. J. et al. Left-handed DNA-PAINT for improved super-resolution imaging in the nucleus. *Nat. Biotechnol.* **39**, 551–554 (2021).
48. Sograte-Idrissi, S. et al. Nanobody detection of standard fluorescent proteins enables multi-target DNA-PAINT with high resolution and minimal displacement errors. *Cells* **8**, 48 (2019).
49. Koch, B. et al. Generation and validation of homozygous fluorescent knock-in cells using CRISPR–Cas9 genome editing. *Nat. Protoc.* **13**, 1465–1487 (2018).
50. Wang, Q., Zheng, B. and Zhang, Y. Example dataset for '4Pi-SIMFLUX: 4Pi single-molecule localization microscopy with structured illumination'. *figshare* https://doi.org/10.6084/m9.figshare.30022948.v1 (2025).

Acknowledgements

We thank L. Gu at the Institute of Biophysics, Chinese Academy of Sciences, for guidance on SIMFLUX data analysis, Q. Xie at Westlake University for sharing the pSin-GFP plasmid and J. Bewersdorf at Yale University for sharing the mCherry-KDEL plasmid. Y. Zhang acknowledges support from the National Key Research and Development Program of China (2022YFC3400600) and the National Science Foundation of China (32150015, 32471516). X.Y. acknowledges support from the 'Pioneer' and 'Leading Goose' R&D Program of Zhejiang (2024SSYS0033). Y.L. is supported in part by the ZJU-UIUC Institute of Zhejiang University. This work was also supported by the State Key Laboratory of Gene Expression, the Westlake Laboratory of Life Sciences and Biomedicine, the Westlake Education Foundation and the Research Center for Industries of the Future at Westlake University.

Author contributions

Y. Zhang conceived the idea and supervised the project. Q.W. designed and built the optical system and performed imaging. B.Z. developed and optimized DNA-PAINT imaging. Z.Y. and Q.D. generated the stable COS-7 cell line of Ensconsin. Z.Y. generated the Nup96 CRISPR cell line. B.Z., Y. Zhan, Q.D. and Y.Q. optimized and prepared biological samples. L.C. and X.Y. prepared the synaptonemal complex samples. Q.W., X.W., S.L. and Y.L. implemented the software and performed data analysis. Y. Zhang, Q.W. and B.Z. wrote the manuscript with input from all authors.

Competing interests

Y. Zhang, Q.W. and B.Z. have filed a patent application on 4Pi-SIMFLUX described in this work. Y. Zhang is co-inventor of a US patent

(US11209367B2) related to the salvaged fluorescence method used in this work. The other authors declare no competing interests.

Additional information

Extended data is available for this paper at https://doi.org/10.1038/s41592-025-02908-8.

Supplementary information The online version contains supplementary material available at https://doi.org/10.1038/s41592-025-02908-8.

Correspondence and requests for materials should be addressed to Yongdeng Zhang.

Peer review information *Nature Methods* thanks Alan M. Szalai and the other, anonymous, reviewer(s) for their contribution to the peer review of this work. Primary Handling Editors: Rita Strack and Nina Vogt, in collaboration with the *Nature Methods* team.

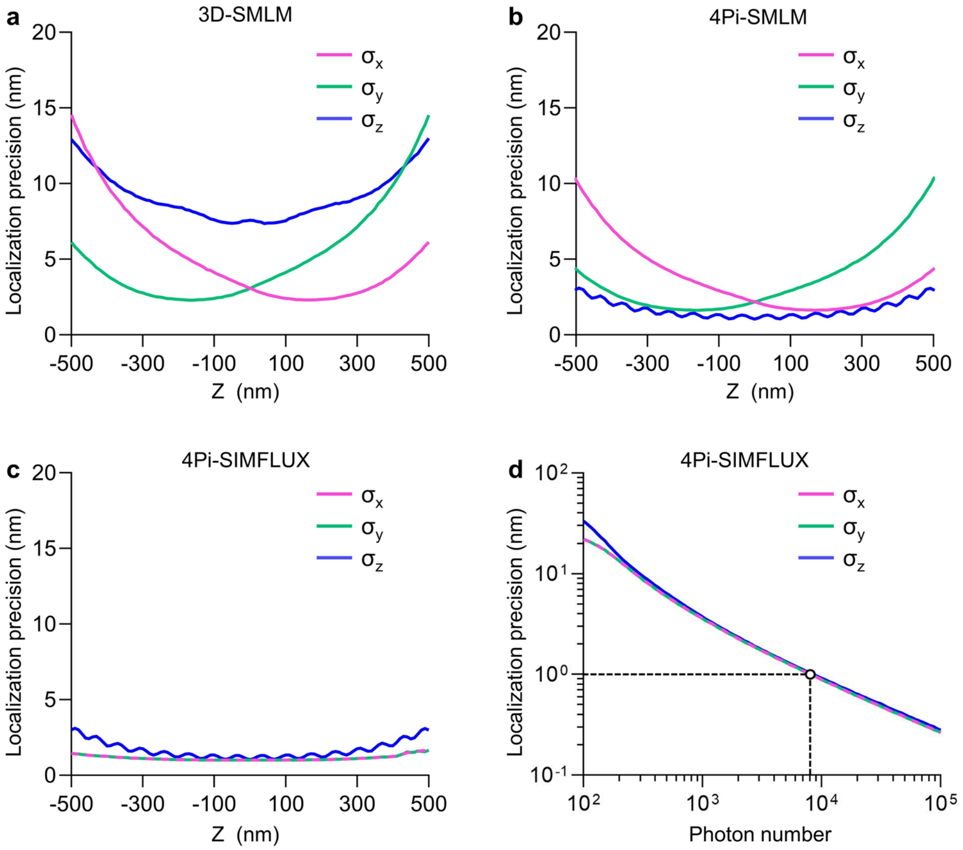

Extended Data Fig. 1 | Performance comparison of 3D-SMLM, 4Pi-SMLM, and 4Pi-SIMFLUX. a-c, Side-by-side comparison of localization precision for 3D-SMLM (**a**), 4Pi-SMLM (**b**), and 4Pi-SIMFLUX (**c**). **d**, Localization precision of 4Pi-SIMFLUX at the focal plane with different photon numbers. The black dashed line denotes 1 nm localization precision. All three simulation experiments were performed using a vectorial PSF model with identical parameters: objective NA = 1.35; medium refractive index = 1.406; emission wavelength = 600 nm; pixel size = 120 nm. For 3D localization and phase-wrapping, an astigmatism of 60 nm in amplitude (root mean square error) was introduced to the pupil function to generate PSFs with elliptical patterns. For 3D-SMLM, the photon count was 4,000 per image with a background of 12 photons per pixel. For 4Pi-SMLM, the photon count was 2,000 per phase image (total of 8,000 photons) with a background of 24 photons per pixel. For 4Pi-SIMFLUX, the 2,000 photons in each phase image were distributed among the six sub-images according to the corresponding excitation patterns (total of 8,000 photons) with a background of 24 photons per pixel. Only Poisson noise was considered. The 4Pi-SIMFLUX illumination pattern was simulated with a modulation depth of 0.9 and an interference period of 210 nm, mimicking experimental conditions. For each z position in all images, 50,000 molecules were simulated. Localization precision was calculated as the standard deviation of the estimated positions.

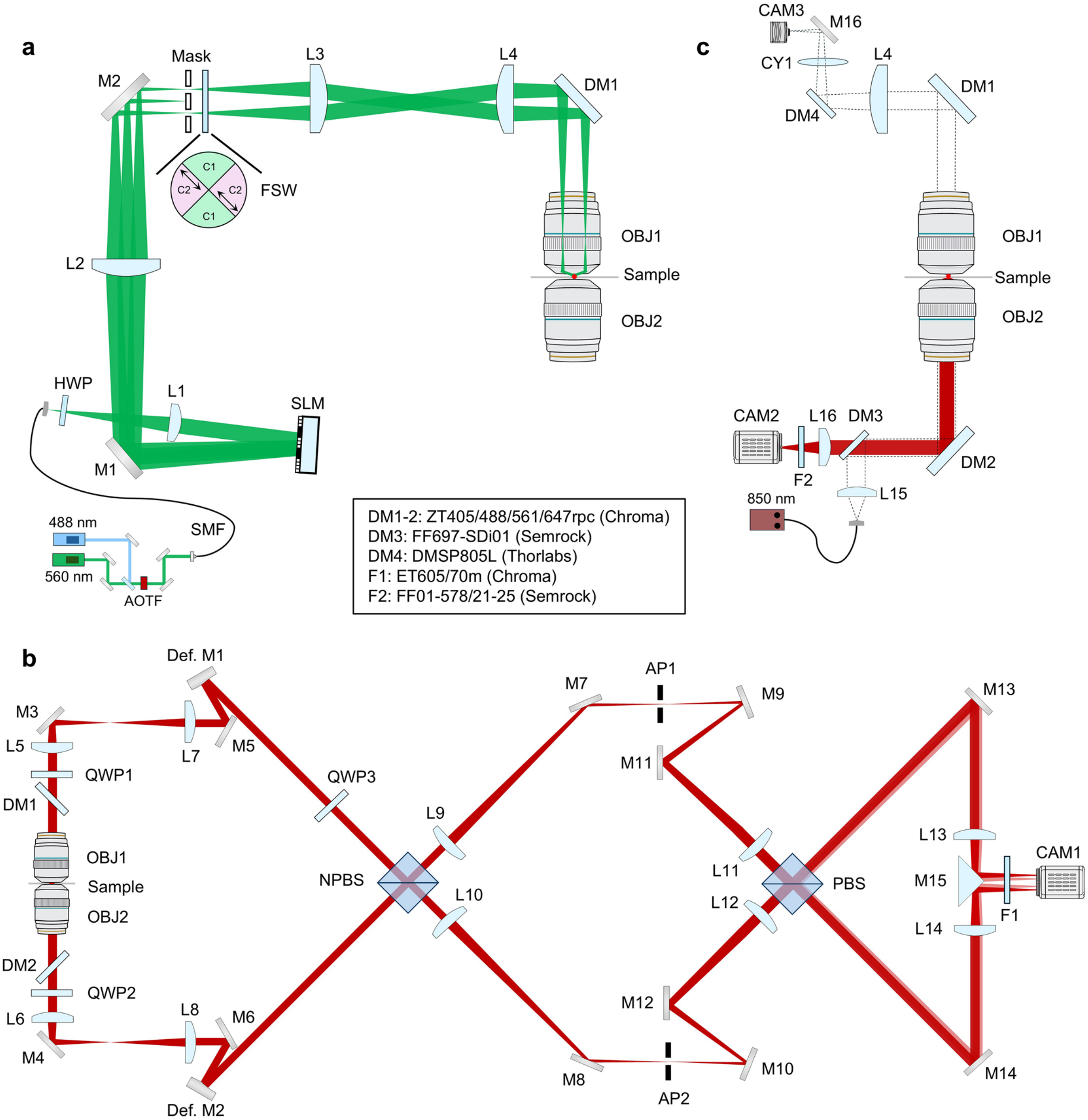

Extended Data Fig. 2 | Optical layout of 4Pi-SIMFLUX. Refer to the **Methods** section for a detailed description. **a**, Structured illumination path. **b**, Fluorescence detection path. **c**, Focus-lock and salvaged fluorescence detection paths. AOTF: acousto-optic tunable filter; SMF: single-mode fiber; HWP: half-wave plate; SLM: spatial light modulator; FSW: four-segmented wave plate; DM1-4: dichroic mirror; QWP1-3: quarter-wave plate; Def. M1, 2: deformable mirror; NPBS: nonpolarizing beam splitter; AP1, 2: aperture; PBS: polarizing beam splitter; F1, 2: emission filter; L1-L16: lens; M1-M16: mirror; CY1: cylindrical lens; CAM1: sCMOS camera; CAM2: EMCCD camera; CAM3: CMOS camera.

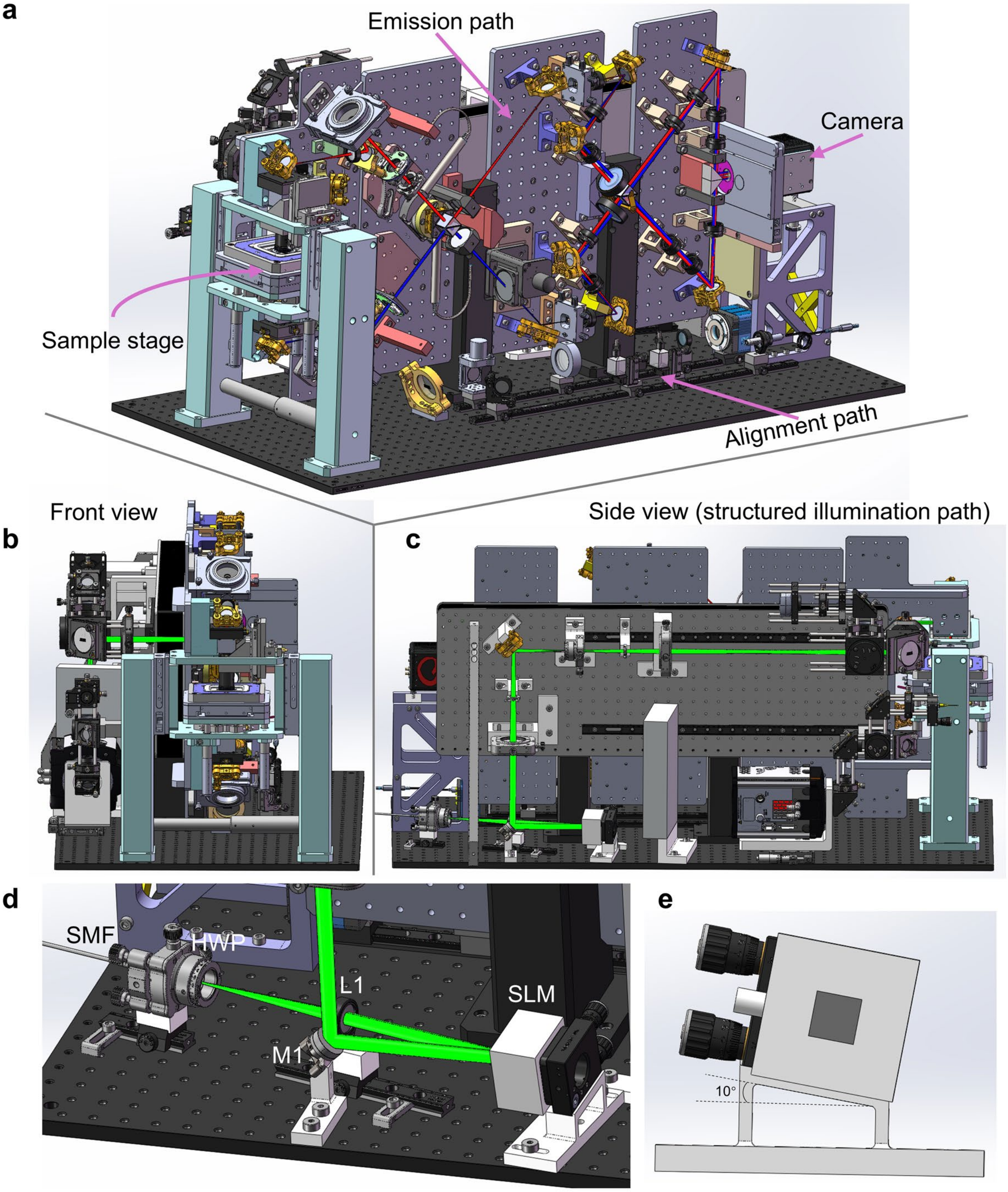

Extended Data Fig. 3 | SolidWorks design of 4Pi-SIMFLUX. a-c, Overview (**a**), front view (**b**), and side view (**c**) of the SolidWorks model of 4Pi-SIMFLUX. **d**, SolidWorks design of the structured illumination path. **e**, SolidWorks model of the SLM mount with a 10° tilt.

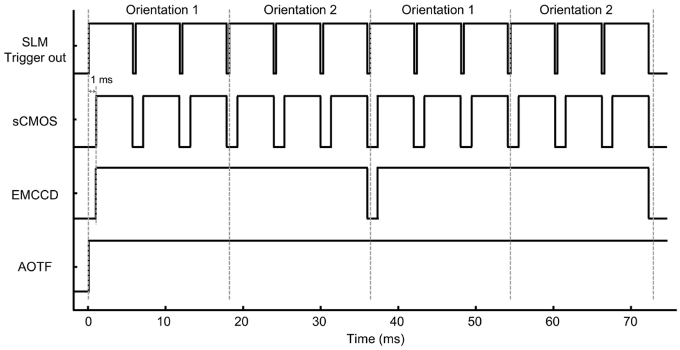

Extended Data Fig. 4 | Synchronization diagram of 4Pi-SIMFLUX. The SLM served as the initial trigger signal, which was transmitted to the sCMOS camera with a 1 ms delay. The EMCCD was triggered once every six sCMOS exposures, and the AOTF remained open. One full 4Pi-SIMFLUX imaging cycle is 36 ms.

https://doi.org/10.1038/s41592-025-02908-8

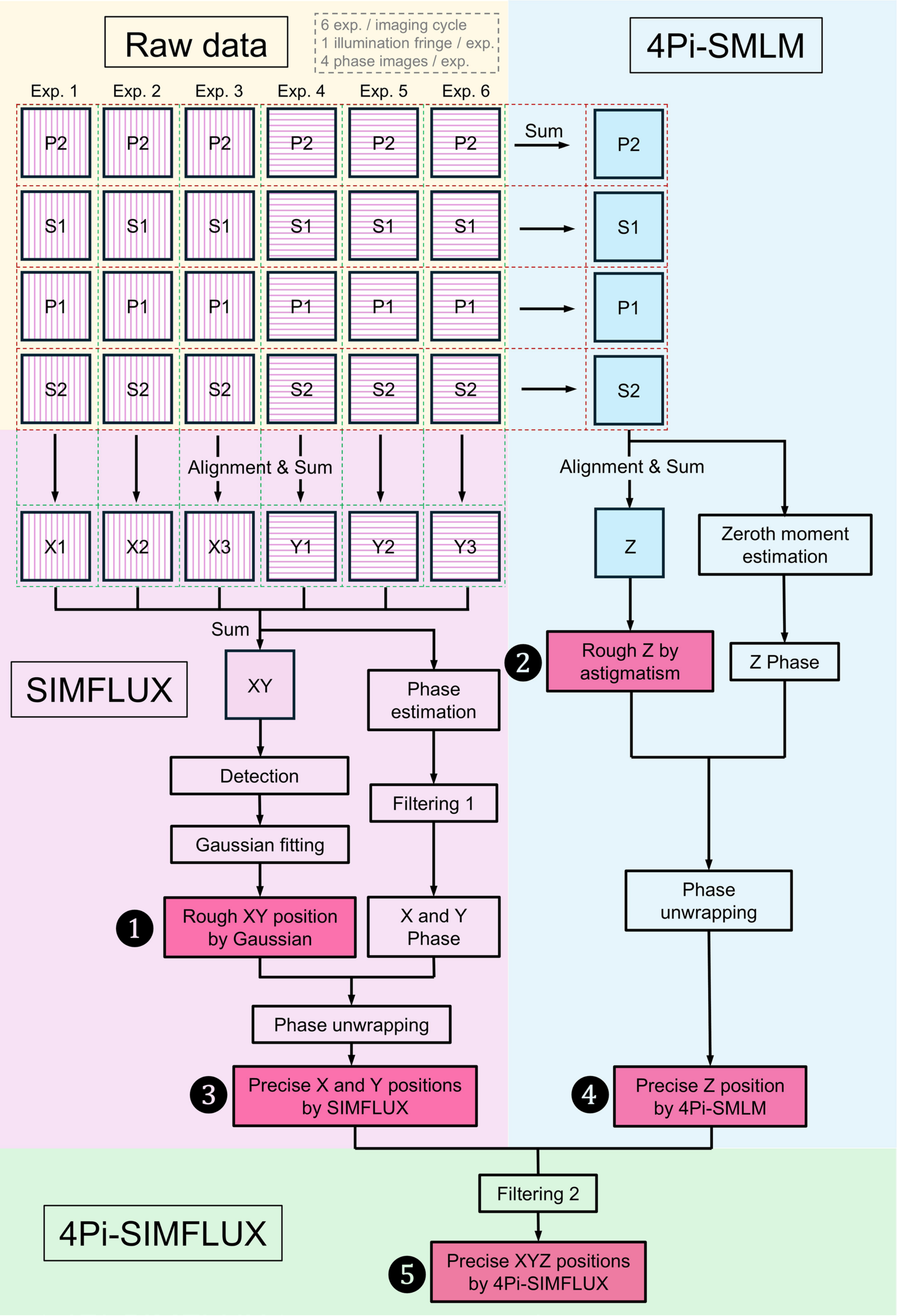

Extended Data Fig. 5 | See next page for caption.

Extended Data Fig. 5 | Algorithm flowchart for 4Pi-SIMFLUX reconstruction. Refer to the **Methods** section and Supplementary Note 2 for a detailed description. Rough XY ① and Z positions ② were estimated by MLE fitting with an elliptical Gaussian PSF model. 4Pi-SIMFLUX integrates SIMFLUX's precise XY positions ③ and 4Pi-SMLM's precise Z position ④ to obtain precise XYZ positions ⑤. In filtering step 1, molecules that are not fluorescent in all six frames were rejected using two filters: photon asymmetry ratio and modulation depth. In filtering step 2, molecules were rejected using other filters such as photon number, localization precision and interference contrast. Please see Supplementary Table 2 and Supplementary Note 2 for details.

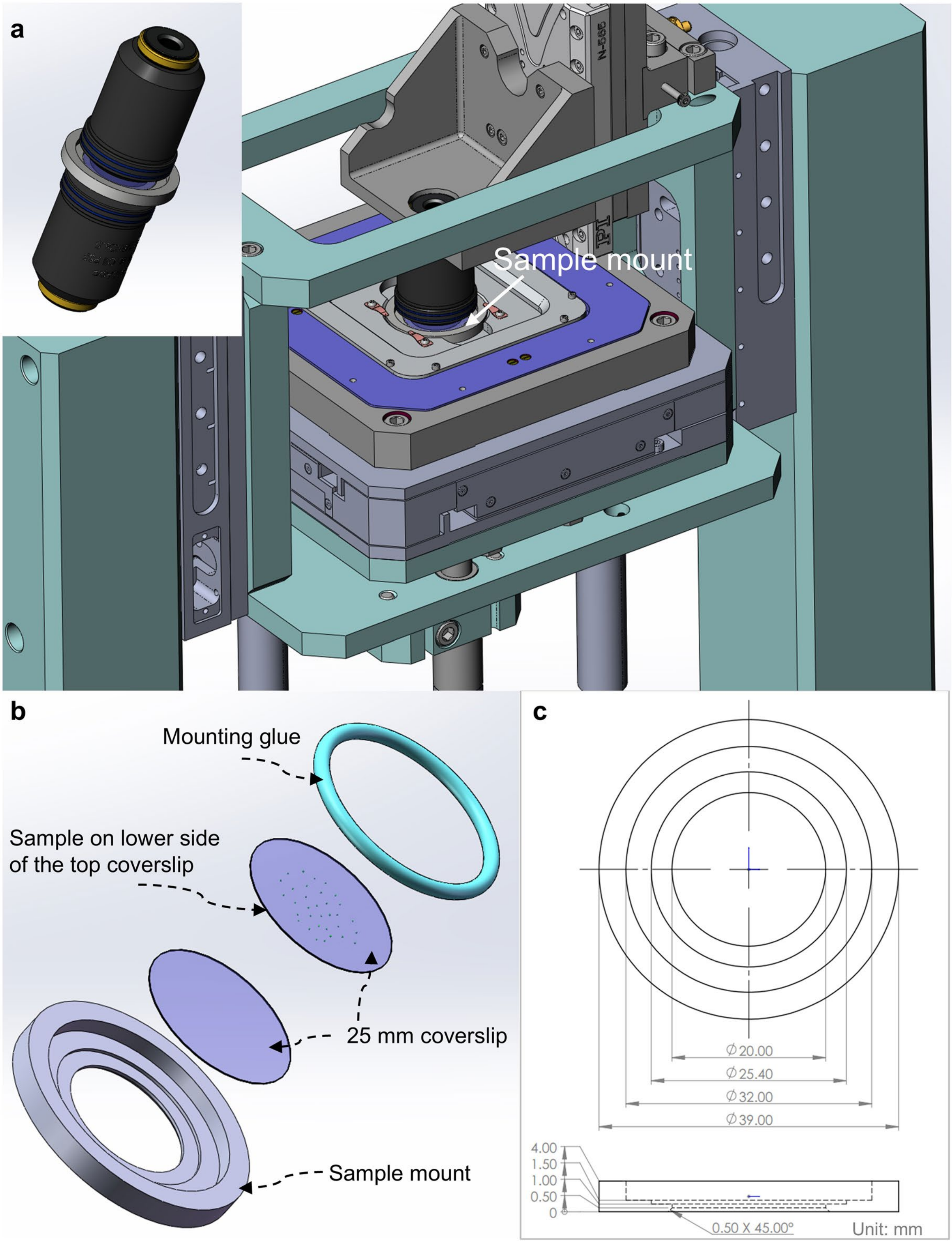

Extended Data Fig. 6 | Sample mounting for 4Pi-SIMFLUX. **a**, Overview of sample mounting in 4Pi-SIMFLUX. The upper left picture shows the sample mounting between the two objectives. **b**, Exploded view of the sample holder and coverslip assembly. **c**, Blueprint of the sample mount.

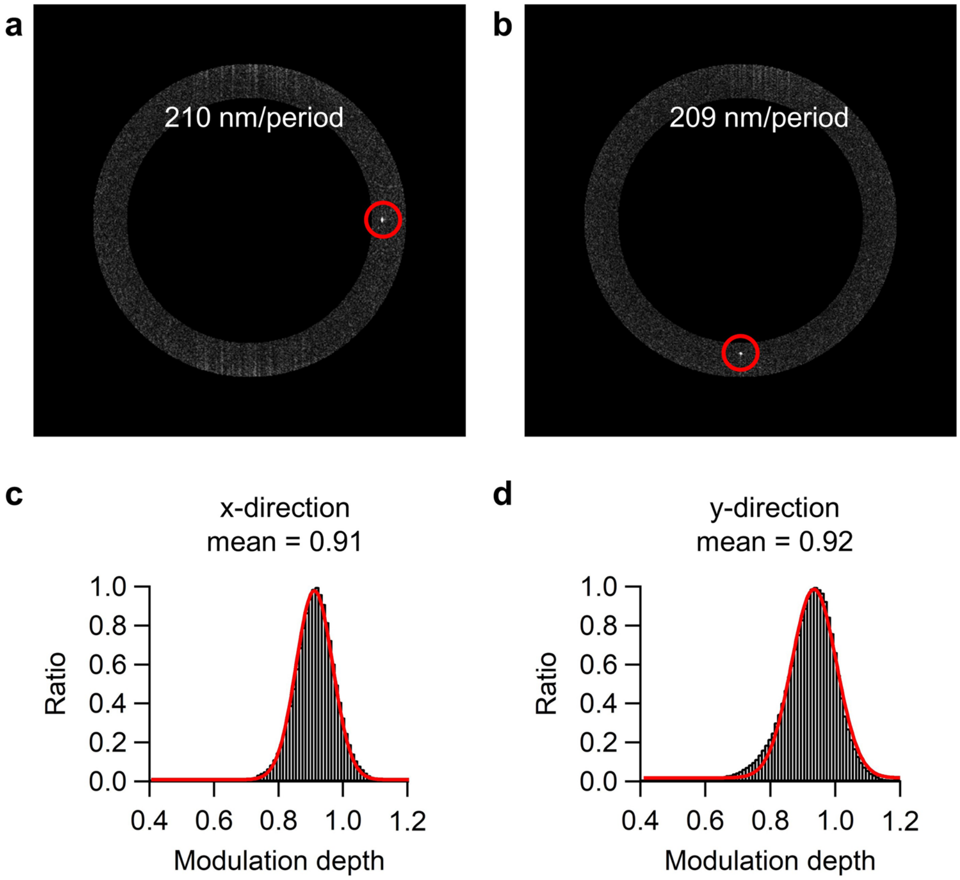

Extended Data Fig. 7 | Illumination grating periods and modulation depth of 4Pi-SIMFLUX. a,b, The cross-correlation spectrum of the 0th and +1st order components in the x- or y-direction. The white dots within the red circles indicate the wavevector's magnitude and orientation of the structured illumination, corresponding to the illumination grating periods of 210 nm (x-direction) and 209 nm (y-direction), respectively. **c,d**, Experimental modulation depths estimated from single molecules in the dataset shown in Fig. 3a are 0.91 and 0.92 in the x- or y-direction, respectively.

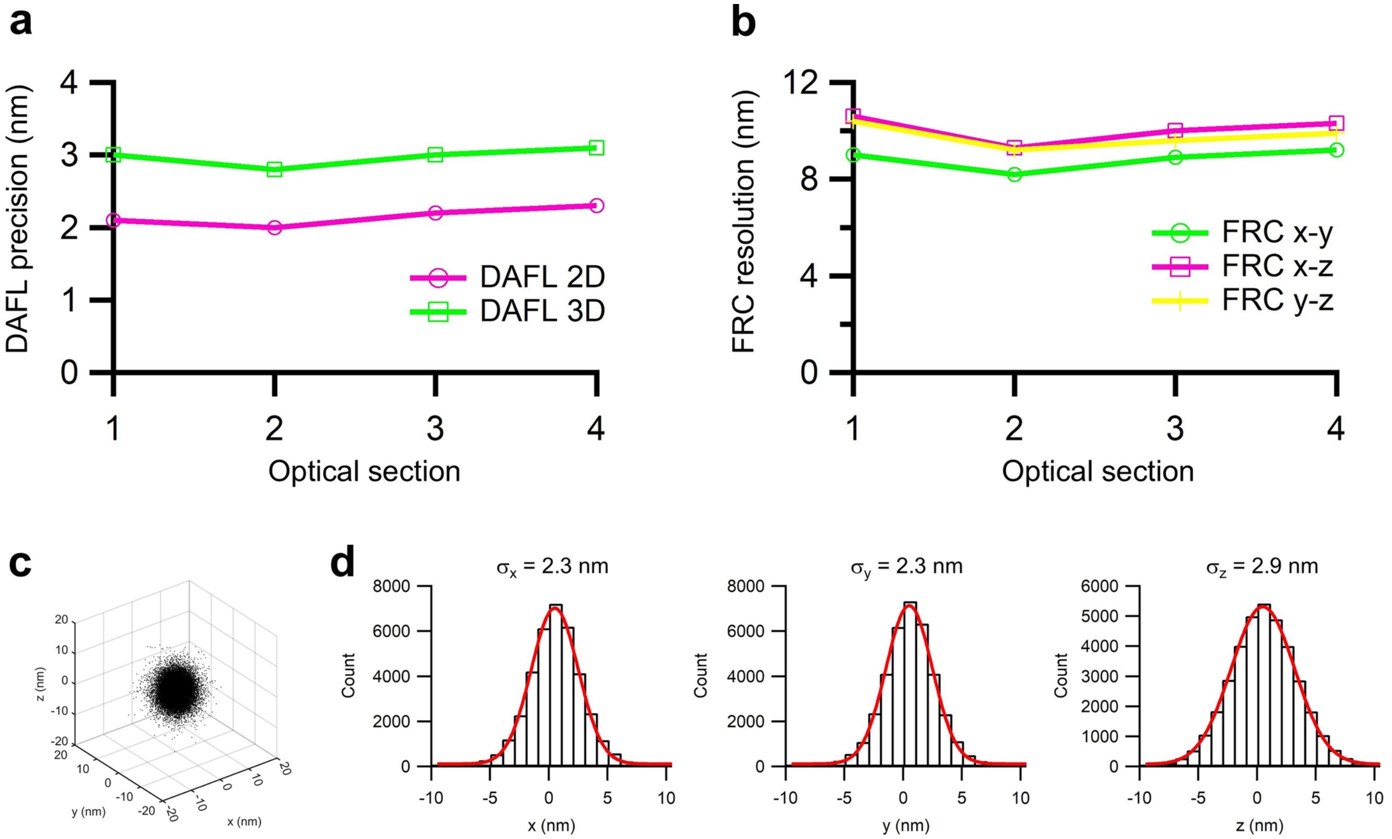

Extended Data Fig. 8 | Resolution analysis for 4Pi-SIMFLUX in mitochondria imaging. The mitochondria image shown in Fig. 5d was reconstructed from four optical sections. **a**, DAFL precision of molecules from each optical section. **b**, FRC resolution for each optical section. **c**, Distributions of 3D localization results from molecules emitting ≥10 frames. The photon count for these molecules is 4,478 ± 1,631 (mean ± s.d.). **d**, Histograms of the distributions in **c** were fit with Gaussian functions, and the standard deviations are reported.

nature portfolio

Corresponding author(s): Yongdeng Zhang

Last updated by author(s): Sep 4, 2025

Reporting Summary

Nature Portfolio wishes to improve the reproducibility of the work that we publish. This form provides structure for consistency and transparency in reporting. For further information on Nature Portfolio policies, see our Editorial Policies and the Editorial Policy Checklist.

Statistics

For all statistical analyses, confirm that the following items are present in the figure legend, table legend, main text, or Methods section.

n/a	Confirmed	
☐	☒	The exact sample size (*n*) for each experimental group/condition, given as a discrete number and unit of measurement
☒	☐	A statement on whether measurements were taken from distinct samples or whether the same sample was measured repeatedly
☒	☐	The statistical test(s) used AND whether they are one- or two-sided *Only common tests should be described solely by name; describe more complex techniques in the Methods section.*
☒	☐	A description of all covariates tested
☒	☐	A description of any assumptions or corrections, such as tests of normality and adjustment for multiple comparisons
☒	☐	A full description of the statistical parameters including central tendency (e.g. means) or other basic estimates (e.g. regression coefficient) AND variation (e.g. standard deviation) or associated estimates of uncertainty (e.g. confidence intervals)
☒	☐	For null hypothesis testing, the test statistic (e.g. *F*, *t*, *r*) with confidence intervals, effect sizes, degrees of freedom and *P* value noted *Give P values as exact values whenever suitable.*
☒	☐	For Bayesian analysis, information on the choice of priors and Markov chain Monte Carlo settings
☒	☐	For hierarchical and complex designs, identification of the appropriate level for tests and full reporting of outcomes
☒	☐	Estimates of effect sizes (e.g. Cohen's *d*, Pearson's *r*), indicating how they were calculated

Our web collection on statistics for biologists contains articles on many of the points above.

Software and code

Policy information about availability of computer code

Data collection	Data collection was performed using custom code written in LabVIEW 2020 (National Instruments).
Data analysis	Data analysis was performed using custom code written in MATLAB R2022b (MathWorks). The code is avalible at https://github.com/zhanglab-srm/4Pi-SIMFLUX. Vutara SRX software 7.0.06 (Bruker) was used for rendering images and videos. Fiji 1.54f was used to crop images, generate line profiles, and perform similar tasks.

For manuscripts utilizing custom algorithms or software that are central to the research but not yet described in published literature, software must be made available to editors and reviewers. We strongly encourage code deposition in a community repository (e.g. GitHub). See the Nature Portfolio guidelines for submitting code & software for further information.

Data

Policy information about availability of data

All manuscripts must include a data availability statement. This statement should provide the following information, where applicable:

- Accession codes, unique identifiers, or web links for publicly available datasets
- A description of any restrictions on data availability
- For clinical datasets or third party data, please ensure that the statement adheres to our policy

An example dataset is available at https://doi.org/10.6084/m9.figshare.30022948.v1. Due to the extensive size of the raw data (> 1 TB per cell, >50 TB in total), uploading it to an online repository is currently impractical. However, the datasets generated and/or analyzed during the current study are available from the corresponding authors upon request.

Research involving human participants, their data, or biological material

Policy information about studies with human participants or human data. See also policy information about sex, gender (identity/presentation), and sexual orientation and race, ethnicity and racism.

Reporting on sex and gender	*Use the terms sex (biological attribute) and gender (shaped by social and cultural circumstances) carefully in order to avoid confusing both terms. Indicate if findings apply to only one sex or gender; describe whether sex and gender were considered in study design; whether sex and/or gender was determined based on self-reporting or assigned and methods used.* *Provide in the source data disaggregated sex and gender data, where this information has been collected, and if consent has been obtained for sharing of individual-level data; provide overall numbers in this Reporting Summary. Please state if this information has not been collected.* *Report sex- and gender-based analyses where performed, justify reasons for lack of sex- and gender-based analysis.*
Reporting on race, ethnicity, or other socially relevant groupings	*Please specify the socially constructed or socially relevant categorization variable(s) used in your manuscript and explain why they were used. Please note that such variables should not be used as proxies for other socially constructed/relevant variables (for example, race or ethnicity should not be used as a proxy for socioeconomic status).* *Provide clear definitions of the relevant terms used, how they were provided (by the participants/respondents, the researchers, or third parties), and the method(s) used to classify people into the different categories (e.g. self-report, census or administrative data, social media data, etc.)* *Please provide details about how you controlled for confounding variables in your analyses.*
Population characteristics	*Describe the covariate-relevant population characteristics of the human research participants (e.g. age, genotypic information, past and current diagnosis and treatment categories). If you filled out the behavioural & social sciences study design questions and have nothing to add here, write "See above."*
Recruitment	*Describe how participants were recruited. Outline any potential self-selection bias or other biases that may be present and how these are likely to impact results.*
Ethics oversight	*Identify the organization(s) that approved the study protocol.*

Note that full information on the approval of the study protocol must also be provided in the manuscript.

Field-specific reporting

Please select the one below that is the best fit for your research. If you are not sure, read the appropriate sections before making your selection.

☒ Life sciences ☐ Behavioural & social sciences ☐ Ecological, evolutionary & environmental sciences

For a reference copy of the document with all sections, see nature.com/documents/nr-reporting-summary-flat.pdf

Life sciences study design

All studies must disclose on these points even when the disclosure is negative.

Sample size	This is a method paper describing the development of the technology,no statistical method was used to predetermine sample size. No sample size calculations were performed. Typically, three to five independent experiments were performed. The sample size was chosen to fully demonstrate the technical performance of our instruments.
Data exclusions	Qualitative exclusion criteria for accepting or rejecting imaged samples were pre-established based on comparisons to previously published images and preliminary experiments performed during the optimization process of the method development. Localized molecules were rejected based on the parameters shown in Supplemtary Table 2.
Replication	The system was aligned daily using fluorescent beads to ensure a good interference before imaging. All attempts at replication were successful. The number of independent experiments were provided in the figure legends.
Randomization	Randomization was not relevant to this study, since no experimental group was formed.
Blinding	Blinding was not necessary, as data collection and analysis were performed automatically using custom-developed software.

Reporting for specific materials, systems and methods

We require information from authors about some types of materials, experimental systems and methods used in many studies. Here, indicate whether each material, system or method listed is relevant to your study. If you are not sure if a list item applies to your research, read the appropriate section before selecting a response.

Materials & experimental systems

n/a	Involved in the study
☐	☒ Antibodies
☐	☒ Eukaryotic cell lines
☒	☐ Palaeontology and archaeology
☐	☒ Animals and other organisms
☒	☐ Clinical data
☒	☐ Dual use research of concern
☒	☐ Plants

Methods

n/a	Involved in the study
☒	☐ ChIP-seq
☒	☐ Flow cytometry
☒	☐ MRI-based neuroimaging

Antibodies

Antibodies used	sdAb anti-ALFA (clone 1G5; NanoTag Biotechnologies, Cat. No. N1502, Lot No. 15220402), sdAb anti-GFP (clone 1H1; NanoTag Biotechnologies, Cat. No. N0302, Lot No. 022307), mouse anti-SCP-3 (clone D-1; Santa Cruz Biotechnology, Cat. No. sc-74569, Lot No. J2221; used at 1:1000 dilution), and secondary goat anti-mouse antibodies (Jackson ImmunoResearch, Cat. No. 115-005-146, Lot No. 171417).
Validation	The nanobodies (sdAb anti-ALFA and sdAb anti-GFP) and antibodies used for labeling were conjugated to DNA-PAINT docking strands and selected based on their validation in previous studies. The specific reagents included sdAb anti-ALFA (doi.org/10.1038/s41467-019-12301-7) and sdAb anti-GFP (doi:10.3390/cells8010048). The primary antibody was a mouse anti-SCP-3 (D-1) monoclonal, raised against amino acids 1-254 of the full-length mouse protein (doi.org/10.1038/s41592-024-02515-z). The secondary antibody was a goat anti-mouse IgG, also previously validated for this application (doi.org/10.1038/s41592-022-01464-9).

Eukaryotic cell lines

Policy information about cell lines and Sex and Gender in Research

Cell line source(s)	COS-7 (CRL-1651), HeLa(CCL-2), U-2 OS (HTB-96) , Sk-MEL-28 (HTB-72) and HEK293T(CRL-3216) cell lines were originally from ATCC.
Authentication	All cell lines were authenticated by ATCC.
Mycoplasma contamination	All cell lines utilized in this study were routinely tested and confirmed to be free of mycoplasma contamination.
Commonly misidentified lines (See ICLAC register)	No commonly misidentified cell lines were used in the study.

Animals and other research organisms

Policy information about studies involving animals; ARRIVE guidelines recommended for reporting animal research, and Sex and Gender in Research

Laboratory animals	Male C57BL/6J mice (JAX, 000664) were laboratory bred or purchased from the animal source center at Westlake University. All experimental procedures were approved by the Institutional Animal Care and Use Committee (IACUC) at Westlake University. Mice were housed in a specific pathogen-free facility at the Laboratory Animal Center of Westlake University. Environmental conditions were carefully controlled and monitored, maintaining a standard 12-hour light/dark cycle, ambient temperature between 22-26 °C, relative humidity levels of 40-70%, and continuous access to standard laboratory food and water. The spermatocyte samples were obtained from the testes of 3-week-old mice.
Wild animals	No wild animals were used in the study.
Reporting on sex	In this study, male mice were used to prepare synaptonemal complex samples.
Field-collected samples	No field collected samples were used in the study.
Ethics oversight	Mice were used and maintained in accordance with the Institutional Animal Care and Use Committee (IACUC) guidelines of Westlake University.

Note that full information on the approval of the study protocol must also be provided in the manuscript.

Plants

Seed stocks	*Report on the source of all seed stocks or other plant material used. If applicable, state the seed stock centre and catalogue number. If plant specimens were collected from the field, describe the collection location, date and sampling procedures.*
Novel plant genotypes	*Describe the methods by which all novel plant genotypes were produced. This includes those generated by transgenic approaches, gene editing, chemical/radiation-based mutagenesis and hybridization. For transgenic lines, describe the transformation method, the number of independent lines analyzed and the generation upon which experiments were performed. For gene-edited lines, describe the editor used, the endogenous sequence targeted for editing, the targeting guide RNA sequence (if applicable) and how the editor was applied.*
Authentication	*Describe any authentication procedures for each seed stock used or novel genotype generated. Describe any experiments used to assess the effect of a mutation and, where applicable, how potential secondary effects (e.g. second site T-DNA insertions, mosiacism, off-target gene editing) were examined.*